P78-2 SATELLITE AND PAYLOAD RESPONSES TO ELECTRON BEAM OPERATIONS ON MARCH 30, 1979

H. A. Cohen[1], R. C. Adamo[2], T. Aggson[3], A. L. Chesley[1], D. M. Clark[4], S. A. Damron[2], D. E. Delorey[5], J. F. Fennell[4], M. S. Gussenhoven[5], F. A. Hanser[6], D. Hall[4], D. A. Hardy[1], W. B. Huber[1], I. Katz[7], H. C. Koons[4], S. T. Lai[5], B. Ledley[3], P. F. Mizera[4], E. G. Mullen[1], J. E. Nanevicz[2], R. C. Olsen[8], A. G. Rubin[1], G. W. Schnuelle[7], N. A. Saflekos[5], M. F. Tautz[9], and E. C. Whipple[8]

ABSTRACT

On March 30, 1979 an electron gun was operated on the P78-2 Satellite. The gun was operated on the satellite before the satellite entered eclipse and during the time of eclipse. The ranges of ejected electron currents and energies were from 0.1 mA to 13 mA, and 0.3 keV to 3 keV. Spacecraft frame, and surfaces on the spacecraft, went positive with respect to points 50 meters from the satellite when the gun was operated. Depending on ejected electron currents and energies, spacecraft frame-to-ambient-plasma potential differences between several volts and 3 kV were generated. Simultaneously, lower potential differences were created between the satellite and a point 3 meters from the satellite. Sample surface potentials were measured during gun operations. When the electron gun was turned off, the vehicle frame swung sharply negative.

Arcing was detected by pulse monitors in several electron beam modes of operation. The ejection of a beam of 6 mA of 3 keV electrons caused three distinct payload failures and created a transient problem in the telemetry system. An attempt has been made to determine the exact time, nature, and cause of these failures; a specific effort has been made to identify which components failed and why they failed. Analytical and modeling techniques have been used to examine possible spacecraft and payload responses to the electron beam ejection which might have contributed to the arcing and payload failures.

---

1 Air Force Geophysics Laboratory
2 SRI International
3 Goddard Space Flight Center, NASA
4 The Aerospace Corporation
5 Boston College
6 Panametrics, Inc.
7 Systems, Science and Software, Inc.
8 University of California, San Diego
9 Radex Laboratory, Inc.

INTRODUCTION

On March 30, 1979, the SC4-1 payload (electron gun) on the P78-2 satellite was operated for the first time to eject beams of energetic electrons from the spacecraft. A wide dynamic range of electron currents and energies was available and was used to charge the spacecraft frame positive with respect to ambient plasma. The use of SC4-1 caused a number of interesting scientific and engineering results. Some of these results were unexpected and some not only unexpected but quite undesirable. In this latter class are the failure of two instruments and a momentary interruption of the normal telemetry stream caused by the ejection of 6 mA of 3 keV electrons.

The first half of this paper will report on the operating modes of the SC4-1 payload, the resultant charging of spacecraft frame and sample materials on the spacecraft exterior and transient pulses recorded. The second half of this paper will present a detailed engineering analysis of the instrument failures and of the telemetry interruption, and a summary of the investigation into possible causes of these problems. As can be seen by the list of coauthors, this paper is the result of contributions and cooperation by a large number of individuals. This paper reports the results from the initial investigation; further conclusions will be published in later reports.

INSTRUMENT PLACEMENT

The P78-2 payloads to be discussed and their positions on the spacecraft are listed in tables 1 and 2 and are shown schematically in figures 1 and 2. For a more complete description of the payloads and the P78-2 spacecraft, see reference 1.

Part of the analysis of the events of pass 89.4 requires a knowledge of the directions of the instruments, defined as "look-angles" relative to the Space Vehicle Relative Coordinates (SVRC). The SVRC are defined such that the forward Omni antenna is the +X axis and the SC-11 boom is the -Y axis (figure 1). The "look-angles" are the two rotations necessary to align the +Z axis of the SVRC to the instrument Line-Of-Sight (LOS). The rotations are: Alpha, a rotation about the +X axis (positive angles being a displacement from +Z towards -Y), and Beta, a rotation about the displaced +Y axis (positive angles being a displacement from +Z towards +X). Both "look-angles" are defined relative to the +Z axis. (Note: In table 2, the "look-angle" of a boom is defined by the axis of the boom, not by an instrument on the boom.)

OPERATIONS SUMMARY

Real time operations for this pass started at Universal Time (UT) 52971 seconds and stopped at UT 57594 seconds. Table 3 and figure 3 outline the operations of SC4-1 for this time period. At the beginning of operations the spacecraft was at 31,000 kilometers altitude, -7.5 degrees latitude, 116 degrees longitude. At the end of operations the spacecraft was at 33,000 kilometers, -7.7 degrees latitude, 119.8 degrees longitude. (A detailed summary of the magnetospheric environment for this pass is included as Appendix 1.) Payload commanding started after the transmitter was turned on and housekeeping instructions were given. A block command was given turning off most of the payloads prior to any SC4 operations. (This is normal safety operating procedure.) The SC2-1 and SC2-2 probes were then turned back on and the 100 kohm shunt which connected the outer surface of the SC2 probe to spacecraft frame was disconnected.

Commands initializing SC4-1 were then sent. These initialization commands set the state for SC4-1 operations but do not turn SC4-1 power on. The power to SC4-1 was turned on and two-and-one-half minutes later the electron beam was turned on. At this time the cap to the electron gun was still in place and no electrons were ejected. The beam inside the closed tube was continuous (0.1 mA of 0.3 keV electrons). SC1, the SC2 probes, SC10, SC11, ML12, and the Transient Pulse Monitor (TPM) were operating, while the power to all the other payloads was kept off. The SC4-1 operating condition with cap closed and beam on was maintained for ten minutes. No changes in the operating conditions of any of the payloads that were on were noted in this time period.

At UT 54082 seconds the command was given to remove the cap from the SC4-1 electron tube. Although the microswitch cap position monitor did not show cap opening, the cap current monitor showed that the cap had been removed. Results from ML12-7, the SC2 probes, and SC10 showed that the cap had been opened and that electrons were being ejected from SC4-1.

The energy of the ejected electrons was then increased from 0.3 keV to 1.5 keV and the beam current was increased from 0.1 mA to 1.0 mA. At 54509 seconds, a command was given to change the electron emission from continuous to pulsed. All of the appropriate monitors indicated that the command was received and a pulsed beam was being ejected from SC4-1. Electrons were ejected in 3.9 mS pulses at a rate of 16 pulses per second. The ejected electron energy was then lowered to 0.5 keV and the command was sent to return the beam to a continuous mode. This command was received and successfully executed. The beam remained continuous from this time until the end of the pass.

The beam current was then increased from 1.0 mA to 6.0 mA. The ejected electron energy was increased to 3.0 keV at UT 54728 seconds. It was during this mode (6.0 mA of 3.0 keV electrons) that identifiable problems of payload and telemetry operation occurred. These problems included: damage to the SC2-1 and SC2-2 probes, interruption of the telemetry, switching the

SC11 wideband telemetry signal line filter from 1 Hertz to 5 Hertz, and the elimination of the SC4-1 pulsed mode.

The SC2-1 probe failed between UT 54728 and UT 54730 seconds and the SC2-2 probe failed between UT 54758 and UT 54759. The telemetry interruption started at UT 54736 and lasted for 14 seconds. A switch in the SC11 filter occurred between UT 54720 and UT 54840 seconds.

SC4-1 was commanded out of this 3.0 keV, 6.0 mA mode at UT 54809, when the energy of the ejected electrons was lowered to 1.5 keV. At UT 54820 the ejected current was increased by command to 13.0 mA.

The SC4-1 pulse mode command was given at 54882. The state monitor indicated that the command had been received but the current remained continuous. Several attempts were made during this pass (and subsequent passes) to put SC4-1 into the pulsed mode: all attempts have been unsuccessful.

There were no other difficulties with SC4-1 during pass 89.4. All commands were received and operated on. There were no signs of poisoning of the SC4-1 cathode. SC4-1 was then commanded through a number of different current and energy modes until it was turned completely off at UT 57109. Real time data acquisition for all the payloads was interrupted during an antenna switch (by command) in the period UT 55728 to UT 55771.

The spacecraft entered penumbral eclipse at UT 56004 (total eclipse at UT 56135) and exited total eclipse at UT 59664 (penumbral eclipse at UT 59832): SC4-1 was operating when P78-2 entered penumbral eclipse and was turned off before P78-2 exited eclipse.

In addition to those payloads turned on prior to the start of SC4-1 operations, the Rapid-Scan Particle Analyzer (SC5) was operated for two short periods during SC4-1 operations. After SC4-1 was turned off (just prior to the end of this pass) all the payloads were turned back on to their normal operating states.

VEHICLE POTENTIAL MEASUREMENTS

Prior to pass 89.4, the SC4-2 payload had been used to eject electrons and ions, both separately and together. During these operations a number of instruments had been used to determine the value of the satellite-frame-to-plasma potential difference (Vsc). These instruments included particle analyzers, (SC5 and SC9), and high impedance differential voltage measurements (SC2-1, SC2-2, and SC10).

Due to the danger of flooding the electrostatic channeltrons with energetic electrons, SC9 was not operated during the SC4-1 operating periods on pass 89.4. SC5 was used for limited time periods during the later stages of this pass. The results and importance of the SC2 measurements (the

difference in potential between spheres three meters from the satellite and spacecraft frame) will be presented in detail in a later section.

For this pass the data from the SC10 measurements were used as the primary source of information concerning the effects of electron ejection on the satellite frame potential, Vsc. The particular SC10 measurement used was the value of the difference in potential (V10) between an electrically floating, conducting cylinder and spacecraft frame. The cylinder (20 meters long and 1/4-inch in diameter) is separated from the spacecraft by a kapton-covered 1/4-inch diameter cylinder 30 meters in length. The two cylinders comprise a 50 meter boom (SC10-3). (A similar boom is also extended on the other side of the satellite.) It is assumed that during SC4-1 operations Vsc = -V10. Some corroboration for this assumption is seen in table 4 where the values for Vsc deduced from SC5 and SC10 measurements are compared. It is emphasized that these are two distinctly different types of measurements of spacecraft frame potential. V10(t), the measured SC10 value as a function of time for the entire pass 89.4, is shown in figure 4. Values of Vsc for each of the SC4-1 modes are listed in table 4. The values given are the maximum measured voltages for the given time periods. The maximum values show the best correspondence between sunlight values (which show spin modulations) and eclipse values (which do not).

Three aspects of the response of Vsc and V10 to electron beam energy, Eb, and electron beam current, Ib, will be singled out for attention: Vsc (0,0), values of the spacecraft frame potential before and after SC4-1 operations when there was no electron ejection; Vsc (Ib,Eb), spacecraft frame potential as a function of ejected electron current and energy; and V10 (Ib,Eb,t), the levels of oscillations of the measured potential difference between the floating SC10 cylinder and spacecraft frame.

Figure 5 shows the period UT 53000 to UT 54080 which covers three different SC4-1 modes:

(1) SC4-1 had not yet been started;

(2) The power processor of SC4-1 had been started but no electrons were emitted from the SC4-1 cathode; and

(3) 0.1 mA of 0.3 keV electrons left the SC4-1 cathode but did not leave the payload because the cap to SC4-1 had not yet been removed.

The character of V10(t) remains unchanged for these three modes. There is an oscillation of V10 with a peak negative value of -5.8 volts when the SC10 boom solar angle is near zero and 180 degrees. (The boom solar angle is the angle between the boom axis and the sun line, a vector pointing from the satellite to the center of the sun.) When the cap to SC4-1 was removed, at 54082, 0.1 mA of 0.3 keV electrons were ejected and Vsc quickly swung positive to a value exceeding 200 V. After this, Vsc responded quickly to changes in ejected electron currents (Ib) and energies (Eb).

Table 5 shows that the current required to swing Vsc to a significant fraction of the beam energy lies between 10 and 100 μA: more current is required when the satellite is in sunlight than when it is in eclipse.

There is a saturation effect using the 1.5 keV electrons. The maximum vehicle potential is obtained when the ejected current lies between 1 and 6 mA and decreases when the ejected current is increased above 6 mA. The oscillations in V10 values cease when the vehicle is in eclipse as shown in figure 6.

Before electron ejection Vsc was slightly positive, of the order of 6 V. When the electron ejection was stopped (modes 20, 21, and 23) Vsc was first near zero and then slightly negative. When SC4-1 was finally turned off for this pass, Vsc went to minus 360 V and slowly decayed toward zero, as is partially shown in figure 7. This phenomenon of negative vehicle potentials induced by terminating electron ejection has since been repeated.

SURFACE POTENTIAL MONITOR MEASUREMENTS

It has been suggested that electron emitters be used on satellites to control spacecraft charging. This pass allowed us the opportunity to study the effects of electron emission on materials typically used on spacecraft. Also, in the attempts to determine the causes of the arcing and instrumentation failures during the operation of SC4-1, conjectures are continuously made about the potentials of the P78-2 surfaces. Actual measured potentials of representative sample surfaces can be used to test various hypotheses. Surface potentials and currents through the samples were measured for various materials during this pass. What will be discussed here are values of the potential (iVj) of the front surface of each sample with respect to spacecraft frame. The back surface voltage of each sample was measured using an electrostatic device and iVj was determined on the basis of pre-launch laboratory calibrations.

Values have been determined for the potentials generated by SC4-1 operations as measured on an optical solar reflector (1V3), a floating conducting band (2V4), and samples of aluminized kapton (1V1 and 2V2). The values of iVj depended on sample material, size and position on the spacecraft. The floating reference band (2V4) tracked the potential of the spacecraft frame:

$$2V4 \cong V_{sc}^{2/3}$$

for Vsc > 0.2 kV. For the other materials, iVj remained low until the vehicle became highly positively charged. For the aluminized kapton samples, iVj depended on both the position and on the size of the samples. Large values of iVj were reached by samples on the equatorial band of the

satellite with the largest values occurring on the largest sample, 2V2 (up to a maximum of -1334 V).

As mentioned previously, SC4-1 ejected 6 mA of 3 keV electrons during mode 11, causing problems for the SC2 payloads and the spacecraft telemetry. Table 6 lists values of the front surface potential of several sample materials during this mode. These values should be used as a guide in assigning values to spacecraft and boom surface potentials in attempts to model particle trajectories or surface behavior during this mode. (Kapton was used on the booms; the potential of the solar cells, which comprise the major areas of the spacecraft, was probably close to that of the sample optical solar reflecting samples; and the floating potential of the conducting reference band is close to the floating potential of the SC2 sphere.) As shown in table 6, the potentials of the samples during this mode, although negative with respect to spacecraft frame, were always positive with respect to the ambient plasma. Figures 8 and 9 show that there were sudden shifts in the current through one sample and also a sudden shift in the front surface potential of another sample, coinciding with the failures of the SC2 spheres and the telemetry interruption. This indicates arcing or a response to arcing at these samples.

With the spacecraft in eclipse, measured values of iVj for the aluminized kapton samples showed that the front surfaces of these samples were charged negatively, not only with respect to spacecraft frame, but sometimes even with respect to the ambient plasma.

PULSES

Two separate payloads were devoted to pulse detection on the P78-2 satellite. A description of sensors, positions, and characteristics measured is given in table 7.

With the exception of changes due to vehicle command related pulses, there was no increase in count rate or amplitude of detected pulses when SC4-1 was first turned on or when a beam was generated but kept in the closed tube. When the cap to SC4-1 was removed and a beam of 0.1 mA at 0.3 kev electrons was ejected, there again was no change in pulse rate or amplitude.

When high energy electrons or high currents were ejected, the rate and amplitude of detected pulses increased significantly. Table 8 shows that there was agreement between the TPM and SC1-8B measurements and that there was a monotonic increase in the pulse rate with current when 3.0 keV electrons were ejected. The 1.5 keV electrons did not lead to a significant increase in pulse rate until a current of 13 mA was used. Even at a large current, the pulse amplitude distribution caused by 13 mA of electrons at 1.5 keV was significantly lower than that caused by the lower current of 6 mA of electrons at 3.0 keV (Figures 10 and 11).

Typical pulse shapes on each of the SC1-8B pulse sensors are shown in

Figures 12-15. The pulses on the same sensor tend to have the same shape. This may suggest that the larger discharges are occurring at the same point on the vehicle. Pulses of differing shapes are seen often enough to rule out an instrumental effect on the shapes. From the results of both the surface potential and pulse measurements, the critical potential on spacecraft frame for the creation of differential charging effects on the P78-2 satellite is between 1.5 and 3.0 kV.

SC2-1 AND SC2-2 MEASUREMENTS AND FAILURE

Each SC2 probe consists of a short boom section (2.54 cm diameter, 38 cm long), a 17.8 cm sphere and a shadow stub (2.54 cm diameter, 25 cm long). These three sections are electrically isolated from each other and are all coated with colloidal graphite (Aquadag). As shown in figure 16, each probe is attached to, but electrically isolated from, the end of a 2.52 meter spacecraft boom. The distance between the spacecraft and the center of the sphere is 3 meters.

The difference between the floating potential of each sphere and the spacecraft frame was made by a null measurement. The voltage difference between an internal Faraday cage and the probe surface was sensed and the Faraday cage was driven by a "follower circuit" so that the potential difference was less than 0.01% of the probe voltage relative to the spacecraft frame. The smallest voltage measurable was $\pm$ 0.01 V and the largest was $\pm$ 700 V.

The values of the two probe voltages as a function of time up to mode 11 are shown in Figure 17. The maximum values for each SC4-1 mode are listed in table 9 where they are compared to V10 values. For each SC4-1 mode, the SC2 probe potentials (V2n) are less than the V10 values and the ratio of V2n to V10 decreased monotonically with increasing spacecraft frame potential. Both of these results are consistent with the concept that the SC2 spheres were inside a plasma sheath created by the positively charged satellite.

Up to the time of the start of SC4-1 mode 11, there were no problems with the SC2 probe measurements. Within 1 second of the start of this mode, the SC2-1 probe failed. The SC2-2 probe drifted to an increasingly negative potential for 30 seconds, reaching a maximum negative potential of -550 V and then failed. The time between the two instrument failures is approximately half of the spin period of the satellite.

The positions of the SC2 spheres with respect to the shadow of the satellite, at times of failures, were determined using boom solar angles inferred from the attitude measurements. A summary of these results is shown in figures 18 and 19. For each failure, the instrument in question is approximately 7 degrees from the satellite shadow, going into shadow. Approximately two thirds of the boom was in shadow when each of the failures occurred. The distance from the probe to the closest position

on the boom in shadow was about 1.2 meters. The failure of each of the SC2 probes was nearly coincident with the boom going through a minimum magnetic pitch angle of 13 degrees for SC2-1 and 15 degrees for SC2-2 (figures 20 and 21). (The magnetic pitch angle is the angle between the magnetic vector and the boom axis.)

Table 10 shows tabulations of both sun angle and magnetic pitch angle for SC2, SC4-1 and ML12-7, using the "look-angle" data in table 2. The sun angle data indicates that the X axis of the satellite was between 3.4 and 4 degrees from being normal to the sun line. A three dimensional calculation of the shadowing of the SC2-1 and SC2-2 booms was determined using data on the probe size, boom length, satellite dimensions and tilt. The result shows that neither of the probes had yet reached the shadow of the satellite when they failed. Both, however, were approaching shadow and a significant portion of the boom had been shadowed when failure occurred. The shadowing angles are summarized in table 11.

The data from both the TPM and SC1-8B were compared with the known periods during which the failures and the loss of telemetry sync occurred. The SC2-1 probe returned "good" data at 54727.9 and "bad" data at 54729.9, indicating failure. The data point at 54728.9 was lost, preventing the time of failure from being pinpointed to closer than two seconds from the SC2-1 data alone. The TPM data which was received during second 54730 indicates at least one fairly large pulse and several that exceeded the counting threshold of the high Z (impedance) and low Z detectors. Preliminary analysis of the timing involved in transmitting the TPM data indicates that this data was sampled between 54728.6 and 54729.8. If we assume that the events monitored by the TPM include the SC2-1 failure, this narrows the period of SC2-1 probe failure to about 1 second.

The SC1-8B data is less easy to interpret. This package shows four consecutive seconds of relatively high activity, starting with the data received about 54728.2 (sampled starting at 54727.2). The 3 keV command was given at about 54728.4, indicating that the first second of this period can be disregarded. However, this leaves three seconds of pulses of which none can be specifically identified with the SC2-1 failure.

During both the SC2-1 failure and the loss of telemetry sync, the SC1-8B package was receiving its data from sensor S2 (Harness Wire). During the failure of SC2-2, SC1-8B was sampling sensor S1 (CDU Loop).

The SC2-2 data shows failure between 54757.9 and 54758.9. The only TPM pulse data which appears to span any of this period was received at 54760 and was sampled between 54758.6 and 54759.8. This appears to narrow the region of uncertainty of the time of the SC2-2 failure to the time period between 54758.6 and 54758.9. The SC1-8B package shows a fairly large pulse at 54759.2 (sampled between 54758.2 and 54759.2) which agrees with this time period. Thus it may be said, tentatively, that the SC2-2 failure may have occurred in the 0.3 second period starting at 54758.6, while the SC2-1 failure cannot be isolated to better than 1.2 seconds starting at 54728.6.

SC2-1 AND SC2-2 PROBE FAILURE ANALYSIS

A partial circuit diagram for the SC2-1 and SC2-2 probes is shown in figure 22. Switches 4 and 5 are open in the floating potential mode which was operational when the probes failed. The high-voltage follower circuit is a high input impedance device when operated within its design dynamic range. The output uses six high voltage transistors to share the high voltage from both the +1 kV and the -1 kV supply. The output follows the input to about ± 700 V beyond which the output circuit limits. The relatively low output impedance of the follower, when operating within its dynamic range, drives the inner sphere of the probe (Faraday shield) and a dual range voltage-to-frequency converter (which digitally measures this voltage).

The time plot for the SC2-1 and SC2-2 spherical probe outputs shows that both spherical probes had been sitting close to -350 V with respect to spacecraft frame, for a period of 172 seconds prior to failure. At the time of failure the outputs of the followers rose to approximately +700 V (as measured by the voltage-to-frequency monitor circuit). The exact rise time of the output voltage is not known for either probe because of the low PCM sample rate of the follower output monitor (once per second).

In both probes the high voltage follower circuit must have failed such that the string of six transistors from the output to the +1 kV supply is conducting and cannot be shut off. The differential driver circuit is protected in one direction by diode D2 and Zener Z2 and in the other direction by identical diodes connected in the opposite polarity. The resulting failure output level of approximately +700 V is not necessarily the normal positive limit level of the output stage but could be the result of reduced power supply voltage due to the sustained high current load of the failed circuit. (The supplies were designed for a maximum load of about ± 100 μA.)

The failure mechanism was most likely a high negative input current to the outer sphere. This current had to be large enough and from a high enough potential source to drive the follower to its natural output limit level of -700 V at which point the output voltage no longer follows the input. The input-to-output voltage differential increases until diode D2 and Zener Z3 conduct. The output is then essentially shorted to the input within 10 V. The input current can then drive the output circuit to a more negative potential than limit level.

When the diodes conduct, the follower output capacitor of 1000 pF is added in parallel with the equal value capacitor in the input filter. Since the capacitance in the +1 kV supply at the circuit board is 2000 pF, it can provide a current of at least 100 μA above the supply design of 100 μA for 1 mS and drop only 100 V. Therefore, the output voltage can be dynamically driven by an input current of about 200 μA for less than 1 mS to greater negative value than -1 kV, without appreciably pulling down the positive supply potential. At this point, the string of six tran-

sistors from the output to the -1 kV supply is essentially off, due to the relatively low potential across them in either polarity. If the follower output is driven toward -1.4 kV, the voltage across each of the six series field-effect transistors (from the follower output to the +1 kV supply) approaches the avalanche breakdown potential of about 400 V; that is, a total of 2.4 kV appears across the transistor string. (The actual transistors were tested to 350 V at 50 μA prior to assembly.)

If the transistor breakdown characteristic has a negative resistance, the junction current can increase while the voltage decreases. When the first transistor breaks down, its voltage decreases, further stressing the remaining transistors and causing them to break down in turn until all six are in avalanche. The total current through the transistors need not be very large at this point. If the current density is high enough at any portion of the transistor junction, catastrophic failure in the conducting mode can take place.

At breakdown the follower input and output are essentially connected together with a total capacitance of 2000 pF relative to ground. The +1 kV supply has a 2000 pF capacitor connected to ground. These capacitances are effectively in series across the six transistor string with approximately 2 kV across them. If the breakdown were to fully discharge this capacitance of about 1000 pF, a total charge of 2 μC maximum would be passed through the transistor string. The approximate currents required would be 2 mA in 1 mS to 20 mA in .1 mS.

The following are the requirements for the SC2 failure (table 12):

(1) Sufficient current must have been introduced to the outer sphere to drive the output of the high voltage follower through protective diodes to about -1200 V to -1400 V. Performance tests of the probes using a 13 kV electron gun proved that the probes could shunt 30 μA with the follower output limiting to -700 V. Therefore, the input failure current had to be in excess of this value but need only be in the order of 200 μA since the design current for the transistors at circuit limit level is approximately 100 μA.

(2) The potential of the current source had to be much greater than -1500 V. The electron gun operating potential at the time of failure was 3 kV.

(3) The total charge required to move the 1000 pF capacitors at the follower input and output about 1000 V was 2 μC. At 200 μA the time to move the voltage on 2000 pF is 10 mS; at 2 mA the time becomes 1 mS. In the extreme case of a 3 kV source with unlimited current capability the maximum current into the input would be limited to less than 250 μA by the 10 kohm input resistor. At this current the time to charge the capacitors to 100 V would be of the order of 10 μS.

(4) The charge available to destroy the transistors after breakdown is also about 2 μC. It is stored in the 2000 pF filter capacitor on

the +1 kV supply line, in series with the 1000 pF capacitor at the follower input and output lines which are charged to approximately -1.4 kV.

The day following the probe failures, switch 5 was closed by ground command connecting a 100 kohm shunt from sphere to spacecraft frame. This caused the probe monitor voltage to drop to about +40 V. The equivalent source at the output is then a +700 V supply with a source impedance of about 1.6 Mohms. This is in agreement with the observation of a 3 to 4 V spin modulation (of the failed probe voltage) when the vehicle is in sunlight. Assuming a probe surface of approximately 1000 cm^2 and a photo-emission of 1 nA/cm^2, the photo-current modulation as the vehicle spins (rotating the probes in and out of the shadow of the vehicle body) is in the order of 1 μA. This should produce a voltage modulation of the order of 1.6 V due to the output impedance of 1.6 Mohms in the failed transistor string.

POSSIBLE PROBE FAILURE CAUSES

Either one of two distinctly different processes is thought to be the cause of the SC2 failures during the SC4-1 operations; arcing along the boom to the SC2 sphere, or impact of beam electrons on the SC2 sphere. The attempts to determine the cause of failure have been directed to be consistent with the SC2 failure analysis, including the values listed in table 12. A plausible scenario can be presented for the arcing hypothesis. As expected (and seen from the measurements of the potentials of the sample materials), grounded conductors, floating conductors, and dielectrics did not charge at the same rate during beam operations. These measurements show that there was a large differential charging between surfaces and spacecraft frame when SC4-1 ejected 3 keV electrons. Differential charging should have occurred along the boom during this mode, since the boom was specifically designed to provide alternate sections of conducting and dielectric segments. The differential charging may have been caused or enhanced by beam electrons returning to the spacecraft, and then striking and accumulating on the boom. As the boom went into shadow, the mechanism for removing these electrons (photo-emission) ceased, and could have created higher differential charging between segments of the boom. The recorded pulse rates and amplitudes show that there was significant arcing on the spacecraft exterior. There is, however, no quantitative explanation of the events, or even a localization of the arcs specifically to the booms and the spheres.

One particular mechanism that produces arcing is the breakdown over the surface of a dielectric due to an avalanche of secondary electrons created by the potential gradient along the dielectric (ref. 2). A technique exists for estimating the current, I, released in this type of arc,

$$I = AC\Delta d,$$

where A is the area discharged per unit time, C is the capacitance of the dielectric per unit area and Δd is the decrease in the voltage differential caused by the passage of the discharge wave over the surface of the dielectric.

If the discharge has a width W and speed V, then

$$A = WV.$$

Laboratory measurements have shown for some dielectrics that

$$V \cong 10^6 \text{ cm/sec};$$

$$C = 10 \text{ pF/cm}^2$$

(an extreme value of the capacity of boom surface to spacecraft ground);

$$W = \pi d,$$

where d = 4.8 cm (the boom diameter);

$$I = 0.15A$$

is a current sufficient to have caused the failures. Even if the many assumptions made in this calculation were valid, open questions would include the duration of the discharge and the total charge transferred.

The beam electrons returning to the space vehicle were considered more likely to strike the SC2 spheres than the ejected electrons on their outward path. An estimate of the return current of beam electrons, I_r, can be made from the measurement results (Table 5). Assuming that orbit limited theory can be used (ref. 3) to estimate the return current of plasma electrons of temperature, Θ; and that

$$V_{sc} >> \theta;$$

$$I_r = KV_{sc};$$

where,

$$K = \frac{neA}{(2 \pi m \theta)^{1/2}}$$

(n = plasma electron density, m = electron mass, e = electron charge, and A = spacecraft area).

For two different values of spacecraft potential, Vsc and Vsc',

$$I_r' = I_r \frac{Vsc'}{V_{sc}}.$$

Using values of I_r, Vsc', and Vsc from table 5 for 3 keV electrons, for mode 11 between 2 and 7% of the return current was due to ambient plasma electrons, and therefore between 93 and 98% of the beam electrons returned to the spacecraft. If a substantial part of this return current struck the SC2 spheres, there would have been sufficient current and energy to destroy the SC2-1 and SC2-2 payloads. However, if the current of $6x10^{-3}$A was returned uniformly over the entire 14 M^2 spacecraft area, the current density would have been $4X10^{-4}$ A/M^2, and the current to the 0.1M^2 area spheres would have been $4x10^{-5}$ A. This current is far below that required for the damage (see table 11). Theoretical attempts have been made to determine the current density of the returning beam. These procedures have included analytical approximations, numerical, and "particle pushing" models. These attempts have shown that the space charge of the beam electrons is an important factor in the beam dynamics, and that the excursion of the beam for the SC4-1 mode 11 was more than an order of magnitude larger than the size of the satellite. Because of these factors, calculation of the self-consistent charge density, and particle orbits, with sufficient accuracy to predict the current density of the return beam have proven to be intractable by straightforward simulation. A two dimensional model shows that for mode 11 the space charge in the emitted beam spread the beam further than it propagated, implying an isotropic return beam. During mode 11, ML12-7 measured a maximum return current of $3.6x10^{-8}$ A. ML12-7 has a geometric factor of 4.26 cm^2/ster. If an isotropic flux is assumed at ML12-7, the current flux at the instrument is $5.2x10^{-4}$ A/M^2, which is consistent with an isotropic flux over the entire spacecraft.

SC4-1 PULSE MODE FAILURE

There are several possible causes of the SC4-1 pulse mode failure. A detailed analysis has eliminated all but one possibility, as the others would have to be random component failures not associated with the 3 kV command execution. A negative transient pulse on the timing gate input line could conceivably damage the input circuit of a TTL 54L14 buffer of the SC4-1. This would have to result in an equivalent short to ground at the input. It is not known how a high voltage transient could be injected onto this line since the timing gate line is double shielded with both shields tied to the connector shell at SC4-1 and grounded at the PCM encoder end. The timing gates from redundant encoders are spliced together within the space vehicle harness wiring. The nature of the splice and shield connections are not known.

TELEMETRY ANOMALIES

In addition to the SC2 sphere failures and the SC4-1 pulse mode failure, there was an anomaly in the telemetry bit stream during mode 11 as monitored by the ground receiving station. (See Appendix 2 for a detailed discussion.) The loss of telemetry sync occurred in main frames 25 and 26

at 54736.397 and 54736.522. The TPM shows a fairly small pulse at 54736 which is too soon and a larger pulse at 54738 (sampled between 54736.6 and 54737.8). This appears to be too late but that may be due to an error in the timing analysis. The SC1-8B package shows a few small pulses at 54737.2 which may be considered as the cause of the loss of telemetry sync.

It may be positively stated that the disruption occurred in the PCM encoder accumulator from which the enable gates and shift pulses are generated. It was caused by a gain of counts equivalent to a time period of nine PCM bits, or 1.1 mS. This is equivalent to thirty-six counts at the x4 bit clock input to the encoder from the TDU. This line is the most probable point of noise injection, caused by a discharge, affecting only the accumulator following. This time shift in the encoder accumulator, relative to the time code accumulator, lasted for 106 frames (13.25 seconds) until the master frame sync, on another line from the TDU, resynchronized the encoder accumulator.

At the time of the noise injection, frame sync was lost on the ground due to the shift in time location of the sync pattern at the end of the main frame. Frame sync was also lost at the beginning of the new master frame due to the return shift of the time location of the three-word pattern.

PASS 89.4 CONCLUSIONS

The operation of the SC4-1 electron gun on the P78-2 satellite created a positive potential on spacecraft frame. The ejection of 6 mA of 3 keV electrons caused large differential charging of the spacecraft surfaces, arcing, a telemetry interruption, and failure of the SC2-1 and SC2-2 payloads. In addition, there was a failure of the SC4-1 pulse mode operation. An analysis of circuitry has identified the components that were affected and has established a basis for determining the causes of the problems. Theoretical studies and measurement analyses have focused on two hypotheses: arcing along the boom to the SC2 sphere, and impact of beam electrons on the SC2 sphere. These investigations still leave a great uncertainty as to the destructive mechanism.

APPENDIX 1: THE MAGNETOSPHERIC ENVIRONMENT FOR PASS 89.4 ON MARCH 30, 1979.

I. Overall Conditions: March 28-30, 1979

On March 30, 1979, the SC4-1 electron beam system on board the P78-2 satellite was operated from ~14:43 to 15:52 UT, while the satellite, in near-geosynchronous orbit, was in the local midnight sector at altitudes of 6.1 to 6.3 R_E. At ~15:30 UT the satellite entered eclipse.

During the time of electron beam operations the magnetosphere was in a stable, quiet period, following two days of intense activity. The activity began with a sudden commencement at 8:27 UT on March 28, and was recorded by all stations in the AFGL mid-latitude magnetometer chain (David Knecht, private communication). The sudden commencement can also be seen in the SC5 particle data and in the SC11 magnetic field data on P78-2.

Following the sudden commencement the magnetosphere became and stayed active for 46 hours, until 07 UT on March 30. Figure 23 shows magnetic indices for the three days. The Auroral Electrojet Index (A_E) shows persistent increasing activity from ~150 nT at 08 UT, to >700 nT by 8:30 UT, after which there are impulsive increases in A_E of up to 1400 nT throughout the active period (7 station A_E index provided by C.-I. Meng). Mid-latitude magnetic activity, as measured by Kp, jumped from 4- to 5+ at 09 UT and reached a maximum value of 7- at the end of March 29. D_{st}, indicating ring current growth, remained at near constant levels (~-40 nT) throughout March 28. On March 29, D_{st} decreased steadily, reaching -120 nT at the end of the day, and recovering throughout March 30. Within an hour of the sudden commencement the equatorward boundary of the diffuse aurora, measured by the DMSP (F2) polar orbiting satellite, fell to 58° CGL (Corrected Geomagnetic Latitude) at 20 MLT and 55° CGL at 09 MLT, indicating considerable Earthward motion of the plasma sheet.

Auroral electrojet activity abruptly decreased to less than 100 nT on March 30, following a northward turning of the interplanetary magnetic field, measured at the ISEE3 altitude at 6:30 UT (E.J. Smith, private communication). After this, Kp fell to 1+ and did not exceed 2+ throughout the remainder of the day. For this period A_E was never greater than 250 nT, typically being considerably less. The evening and the morning diffuse auroral boundaries systematically moved poleward over a 6 hour period to upwards of 65° CGL.

During the electron beam operations (from 14 to 16 UT), Kp varied from 2+ to 2-, A_E was less than 170 nT, and D_{st} ~-54 nT. For this period there were two DMSP (F1) optical images of the south polar region, each covering the dusk half of the oval. For the first image the satellite crossed the pole at 14:30 UT, and for the second at 16:10 UT. Each showed a contracted auroral oval with extended, weak arcs. The later image showed the auroral region in the midnight sector to be thinner by several degrees

and less intense, indicating an uninterrupted quieting process. In all, it can be concluded that the state of the magnetosphere was sufficiently quiet and stable throughout the two hour period to justify extrapolation of plasma parameters into the period of beam operations, since these necessarily interrupt many of the measurements of the ambient plasma. The justification applies to extrapolations in time only. We must also be aware of spatial changes which P78-2 may have encountered during this time.

II. The Position of the Satellite in the Magnetosphere.

A. Position with respect to particle populations.

Figure 24 is a schematic diagram of the P78-2 orbit on March 30, in L-shell and in local time (the outer tick marks, with noon at the top of the figure). The tick marks on the orbit itself mark Universal Time. The beginning of March 30 (00 UT) is at dawn. At this time Kp had its highest value for the day, equal to 5. In addition to the satellite orbit, Figure 24 shows boundaries for the two major magnetospheric particle populations: the plasma sheet, a hot, tenuous plasma; and the plasmasphere, a cold, dense plasma. The boundaries are statistically derived, and Kp dependent. The inner edge of the plasma sheet is given by the dashed line, and is taken from a model derived using over 6000 DMSP (F2) auroral oval boundaries (ref. 4). The plasma sheet relaxed outward (away from the Earth) throughout the UT day as activity diminished. (The abrupt changes in the boundary are a result of the 3-hour time intervals of Kp.)

In crossing the plasma sheet an increase in energetic (>50 eV) particles is expected. All increases in energetic particles at near-geosynchronous orbit are, in the literature, somewhat misleadingly referred to as injection events. Plasma sheet crossings are differentiated from other injection events by a clear energy dispersion in the particle flux increases as quasi-stationary Alfvén boundaries for higher energy particles are traversed.

Figure 25 gives the electron number density (in cm^{-3}), energy density (in keV/cm^3) and average energy (in keV) calculated from the electrostatic analyser data of SC5 for March 30. The energy range is from 50 eV to 60 keV; in order to calculate the moments, the distribution functions obtained at a rate of once per second from the detectors parallel to the spin axis are integrated over pitch angle. The closest approach to the magnetic field varies from 45° at 12 UT to 4° at 16 UT. SC5 did not operate for most of the first half of the day and was turned off for the initial electron beam operations near 15 UT. The large spikes in the data delineate the period of beam operations, ending prior to 16 UT.

The plasma sheet crossing occurred at 13.7 UT, almost precisely at the model prediction. The crossing had a clear signature in the number density (sharp increase) and in the average energy (sharp decrease since the zero energy Alfvén layer was crossed first). After the crossing, the number

density remained fairly constant, .35-.5/cm^3 for several hours (extrapolating through the data gap and beam operations), while the average energy increased as higher energy Alfvén layers were crossed. The data gap occurred prior to crossing Alfvén layers for particles with energies greater than 10 keV. The temperature, as measured by the average energy ($3/2kT = \bar{E}$), also increased from 260 eV at the plasma sheet crossing to 1.2 keV at 16 UT. Thus, for electrons with energies less than 10 keV, it appears that there were no major spatial changes during the period of beam operations, while there may have been a systematic increase in the mid-range energies (10-60 keV). The solid state detectors on SC5 showed the electron population for energies greater than this (into the MeV range) to be virtually unchanged throughout the period.

Ions do not show a clear signature for plasma sheet crossings. The corresponding values of the moments of the ion distribution, as measured by SC5 in the same energy range, had regular variations over the two hour period of interest. The number density remained relatively constant between 0.6-0.7/cm^3, and the energy density decreased from 12 keV/cm^3 at 14 UT to 4.8 keV/cm^3 at 16 UT, while the temperature (determined by average energy) decreased from 11 to 6 keV over the same period.

Of great interest in charging operations is the position of the plasmasphere and the encounter of related, warm plasma populations ($kT<30$ eV). The instruments designed to measure the cold component of the magnetospheric plasma (temperatures less than a few eV) failed early in the P78-2 mission (Experiments SC6 and SC7). SC9 measures particles downward in energy to several eV, and therefore, covers a good portion of the warm plasma component (from 1-30 eV). The higher energy spectrum is well-determined into the MeV energy range for both electrons and ions by the combined measurements of SC2-3, SC-5, SC-3, SC-8, and SC-9. The low energy population greatly affects spacecraft charging and beam operations, and the loss of on-board measurement of this component is debilitating, particularly in modeling efforts. At best we can only set upper limits on densities.

The problem of setting limits on the low energy plasma populations for SCATHA operations can be addressed in two ways: (1) from an overall knowledge of plasmaspheric dynamics; and (2) from near-coincident measurements made by other satellites at geosynchronous altitudes.

In brief, previous studies show that the plasmasphere is a region of high density (10-1000/cm^3) warm plasma that corotates with the Earth and whose source is the ionosphere (ref. 5). The plasmasphere can extend to geosynchronous orbit, most typically after prolonged periods of quiet magnetospheric conditions and for local times in the afternoon sector. During active periods the outer regions of the plasmasphere are depleted and are replaced by the Earthward-moving, low-density, hotter plasmasheet. Subsequent filling of the plasmasphere from the ionosphere after the plasmasheet has receded to quiet time positions is generally slow (on the order of tens of hours). Since the period of beam operations was within 10 hours of a very active period, and since P78-2 was very clearly inside

the plasma sheet at this time, we may safely conclude that P78-2 was not in a region of the highest cold plasma densities (100-1000/cm^3).

However, intense (10-100/cm^3) and weak (1-10/cm^3) warm plasma populations can be encountered outside the plasmasphere at geosynchronous orbit (ref. 6). The former are not found in the midnight sector, and the latter only rarely so during times of low magnetic activity. Geos 2, at geosynchronous orbit, lagged P78-2 by about 5 1/2 hours during March 28-30. The superthermal plasma analyser on board detected cold ion densities (T $\sim$1 eV) on March 28, 29 from $\sim$10-20 hours local time (LT) with densities ranging from 1-16/cm^3. The peak densities ($\sim$10/cm^3) occurred between 13:30 and 15:30 LT. On March 30, this population was not detected at these local times but was encountered beginning at 17 LT, reaching a peak value of 8/cm^3 at 21:30 LT and disappearing by 22:30 LT. Field-aligned cold plasma fluxes (with equivalent densities up to 10/cm^3) were encountered from 10 to 21:30 LT (Gordon Wrenn, private communication). Therefore, it can be concluded that the fringes of the plasmaspheric filling process may have been encountered by P78-2 at times near those of beam operations (prior to local midnight). From the Geos 2 data an upper limit to the cold plasma population with temperature $\sim$1 eV can be set at 10/cm^3.

B. Position of the satellite in the magnetospheric magnetic field.

Figure 26 is a schematic diagram showing the position of P78-2 with respect to the magnetic field during beam operations on March 30. The projection is in the meridional plane. The satellite is in the southern hemisphere at a magnetic latitude of -18.6° and a geographic latitude of -7.8°. The magnetic field, measured by SC11 on SCATHA, is in a tail-like configuration, at an angle of only $\sim$30° to the solar direction.

At the time of the SC2 failure, the total magnetic field was 178 nT, decreasing at a uniform rate of 24 nT/hr. In Earth-Centered Inertial coordinates (x parallel to the line of equinoxes and in the direction of the autumnal equinox, z parallel to the polar axis of the Earth's North Pole, and y=zxx) the field components are: B_x = -157 nT, B_y = 16 nT, B_z = 82 nT; that is, the field is nearly meridional, making an angle of 28° with the solar ecliptic. The field remained tail-like throughout the sunlit electron beam operation. At 15:36 UT the field suddenly rotated into a dipolar configuration and remained in this configuration for several minutes. After this the field returned, as suddenly, to a more tail-like configuration (by $\sim$8°) than prior to the rotation. The field begins a slow recovery toward dipolar-like configuration after 15:50 UT. (Note: further investigation is being conducted to support the existence of the anomalously large rotation at 15:36 UT.)

III. Distribution Function of the Ambient Plasma Prior to Beam Operations Using SC2-3 , SC5, and SC9 Measurements.

Three particle detectors, SC2-3, SC5, and SC9, operated on March 30

to within 12 minutes of the time when the cap on the electron beam was removed. The data from these operations (14:45-14:49 UT) are used to calculate an average isotropic distribution function to represent the ambient plasma. The energy range, position on the satellite, energy pass bands and pitch angles differ for the three instruments and thus they do not lend themselves to easy comparison. A comprehensive intercalibration of the P78-2 instruments is underway. The intercalibration will address the differences cited above, and in addition, differences in calibration methods, degradation in flight, and ion composition. Thus, the distribution function constructed here should be considered preliminary.

Figure 27 is a plot of the distribution functions of electrons and ions for a one minute period in the given 5 minute interval. The breadth in the values for SC2-3 and SC5 result from their pitch angle sampling. The low energy (<10 eV) electrons in one SC9 detector (solid line) and the low energy ions (<10 eV) monitored by SC9 are at background levels.

The ion distribution function is calculated over two energy ranges, <1.5 keV and >1.5 keV. The higher energy range is well-fit up to 188 keV by a Maxwellian distribution with temperature between 14-16 keV, and number density between 0.4-0.6/cm^3. For the low energy (~ .07-1.5 keV) the SC5 counts are at background levels and are omitted from consideration. A Maxwellian distribution is not a particularly good choice for this range, but a reasonable fit is made with temperature and density, 180 eV and .05/cm^3, respectively. A power law distribution gives a much better fit to the low energy SC9 data down to 10 eV. For a power law: $f = f_0 E^{-\alpha}$ sec^3/km^6), $f_0 = 4.38 \pm .13$, $\alpha = -1.6 \pm .1$, and the density is .07/cm^3 to within 20%.

The electron distribution functions for the three instruments differ greatly, although the difference is principally in the value of the function, and not the shape. The electron distribution function here, and as is often found to be the case, does not fit a Maxwellian except for small energy intervals. Therefore, we again fit the data to two non-overlapping power law distributions, one in the energy range .050-5 keV, and one >5 keV. In the low energy range $\alpha = 1.25$, with f_0 varying between 2.4 and 4.37, giving a density variation from .41 to .75/cm^3. In the high energy range $\alpha = 3.2$, $f_0 = 4.95$ and $n = .008$/cm^3. In this last fit, the SC2-3 data was not used. The values are low due to the use of an efficiency factor of unity for all energies. (For the above power laws, E is in keV and f_0 has the same dimensions as f.)

APPENDIX 2: TELEMETRY ANOMALIES

A detailed analysis of the problem and its probable causes has been made. In order to understand the telemetry data anomalies, a description of the Pulse Code Modulator (PCM) output format follows.

All data inputs to the PCM encoder are sampled at least once in a 16 second interval, the time required for one master frame. The master frame consists of 128 main frames. The time for one main frame is then 0.125 seconds. Each main frame consists of 128 words of 8 bits in length, producing a bit frequency of 8192 bits per second.

Several words of each main frame are dedicated to frame identification, synchronization, and vehicle time. This allows for decommutation of the serial digital data when received on the ground and for time-tagging the encoded data. Table 13 is a listing of the binary values of these dedicated words as decommutated from the data tape.

The first four words of the main frame, words 000 through 003, contain the Vehicle Time Code Word (VTCW). Word 000 contains the 8 most significant bits of the binary time code. Words 001 and 002 contain the next 16 most significant bits, and the first 4 bits of word 003 are the four least significant bits of the time code. The remaining four bits of word 003 are a fixed zero ("A", table 13) and a repeat of the three least significant bits of the time code.

The least significant bit of the time code changes every main frame and therefore has a weight of 0.125 seconds. The capacity of the time code accumulator is 2^{28}x0.125 seconds or greater than 388 days. This accumulator and the shift register for the vehicle time code (figure 28) are located in the Timing Distribution Unit (TDU).

Word 124 of the main frame is a main frame binary counter readout. It is synchronized to the master frame and is advanced one count each main frame. In normal operation it is identical to the eight least significant bits of the VTCW. It has a capacity of 128 (000 to 127) which is the number of main frames in a master frame. This counter is located in the PCM encoder. It is important to note that although equal to the last eight bits of the time code, the generation of the frame count is accomplished in a different assembly.

The last three words of the main frame (125, 126, and 127) are dedicated to main frame synchronization. These 24 bits have the octal coding 01147537. This sync code resides in a Read-Only-Memory (ROM) located in the PCM encoder.

The PCM encoder (figure 29) generates all enable gates and gated shift pulses for taking data from payloads and the TDU (for the VTCW). Normally these gates are generated using a x^4 bit clock signal (32768 Hz) and a 1/16 Hz master frame synchronizing signal from the TDU.

If the external clock from the TDU fails, there is a crystal controlled clock internal to the PCM encoder which automatically takes over, providing timing gates, enable gates, shift pulses, and special timing gates for experiments SC4, SC9, and SC11, as well as the main frame counter.

During Pass 89.4 of the P78-2 satellite there was a disruption of the digital data stream from the PCM encoder. This occurred 8 seconds after the 3 keV command execution on the electron gun experiment. The first data from AFSCF showed a 14 second data dropout, a loss of about 105 main frames.

After analyzing the data using a program which recognized the start of the master frame and then counted main frames, it was found that the instrument data was not lost nor was it erratic. Successive instrument data samples showed no serious magnitude jumps. The vehicle time code, however, was invalid for these 105 frames.

Since the time code, frame counter, and synchronzing words either remain constant or advance in a predetermined pattern, the main frame words associated with these functions were examined in detail for the data disruption period. A careful examination of table 13 reveals the following:

(1) Up to frame 025 the data was normal. The VTCW and frame counter were incremented by one each main frame. The frame synchronization remained correct and constant.

(2) During frame 025 at UT 54736.397 (assumed to be the time of the start of frame or the time of frame synchronization), the VTCW (PCM words 000, 001, 002, 003) was normal. By the end of the frame, however, the expected bit locations were nine bits early ("B", table 13); word 124, the frame identification word, is a count of main frames in the master frame, and had a count of 9 instead of the expected 25. This count, 00001001, also happens to be the second through ninth bits expected in the frame synchronization pattern (words 125, 126, 127; "C", table 13).

The first 15 bits in the frame synchronization pattern were the same as those expected during normal operation in the tenth through twenty-fourth bits in these three words. This indicates that the PCM encoder was presenting data to the output nine bits early, starting some time after word 003 but before word 124 of frame 025.

(3) During frame 026 at UT 54376.522 the ground decommutation had not yet found the synchronization pattern and was still sampling at the normal rate. Actually, the decommutation and the VTCW were synchronous but the PCM readout was nine bits early. This means that the shift pulses for the first nine bits of the first word occurred as the last nine bits of the last word of frame 025. Since the VTCW shift register was not loaded at the start of the readout, it shifted out nine ones. (The VTCW shift register shifts in all ones into its front end as it shifts out the time code.) The nine ones at the end of frame 025 are then explained.

Assume that the PCM encoder is nine bits ahead of the VTCW shift register

process. Just before the tenth shift pulse, the VTCW accumulator generated a VTCW shift register load signal and loaded the register with the correct time from the accumulator. The next twenty-three shift pulses shifted out the proper time code, most significant bit first, and then the shift pulses from the encoder to the VTCW shift register ceased. The next nine bit slots were all zeros. This apparently was data from SC2 which fits into the eight bits of word 004 and bit one of word 005 of frame 026.

At the end of frame 026 the frame identification and frame synchronization still exhibited the nine bit advance of the PCM encoder but the last sixteen bits were garbled. This is apparently the time during which the ground decommutator corrects for the shift after recognizing the synchronizing pattern.

(4) In frame 027 at UT 54736.646 note first that the UT is 1 mS faster than expected ("D", table 13). Every second frame time-tag ended in a .xx7 or a .xx2. From this frame until the start of a new master frame the time-tags ended in .xx6 and .xx1. This means that the PCM data string was arriving 1 mS (nine serial data bits) earlier than previously.

The first nine bits of the VTCW do not form an identifiable pattern and can probably be explained by the resynchronizing process in the ground decommutator. However, the last twenty-three bits of the VTCW form the exact pattern expected in the first twenty-three bits of the VTCW. This can only occur if the load signal to the VTCW shift register (in the TDU) occurred nine bits later than the beginning of the VTCW shift operation.

It should also be noted in this frame that the frame counter (word 024) and the frame synchronization pattern (words 125, 126, 127) were correct.

(5) In frame 028, at UT 54736.771, all data except the VTCW were correct. The VTCW bit pattern shows that the first nine bits are the same as those expected during normal operation in the last nine bits of the VTCW in the previous frame ("E", table 13). The ground time-tag is 1 mS fast, as compared with time-tags prior to frame 026 and after frame 001 of the next master frame.

This pattern persists until the beginning of the next master frame; that is, the vehicle time code appears to be nine bits late. Frames 035 through 119, although not printed out in this table, did exhibit this pattern.

(6) At UT 54749.271, the beginning of the next master frame, the pattern changed. The PCM encoder circuits were reset by means of a master external sync signal from the TDU. This signal is a 0.0625 Hz square wave, and synchronization occurs on the negative-going edge of this signal. This is always when the last seven bits of the time code (bits 22 through 28 of the VTCW) go to all zeros, indicating frame count decimal 000. However, in frame 000 of the new master frame, the first twenty-eight bits of the first four words are what would be expected with the nine bit VTCW delay.

The frame sync was lost and the ground decommutation process did not pick up frame sync until frame 014.

(7) A second pass of the tape produced data for main frames 002 through 013, and showed that the VTCW neither lost nor gained time relative to the time before the anomaly began. The ground time-tags were all 1 mS earlier than expected during the anomaly ("F", table 13).

(8) All data patterns were normal from UT 54749.522 onward.

A review of the schematics for relevant circuits resulted in the block diagrams for the Vehicle Time Code Generator located in the TDU (figure 28) and the PCM encoder (figure 29). These diagrams reveal the following:

(1) The TDU sends two timing signals to the PCM encoder which are used in normal operation. These are a x4 bit clock square wave at 32768 Hz, and a 0.0625 Hz square wave. The x4 bit clock is used to generate all word enable gates, shift pulses, frame counts, and addresses for the synchronization ROM. Most of these functions are accomplished in the encoder by means of counters and hard-wired logic.

(2) The VTCW is generated in the TDU. The basic clock used for the time code is the same as that used to generate the x4 bit clock signal sent to the PCM encoder. The VTCW shift register is also located in the TDU. Although the shift enable gate and the gated shift pulses for the VTCW shift register are generated in the encoder, the load signal which transfers data from the clock accumulator stages to the shift register (in a parallel fashion) is generated by circuits in the TDU using clock signals from the clock accumulator.

It is therefore possible for the accumulators in the TDU (which generate the VTCW) and the accumulators in the PCM encoder (which generate the enable gates and shift pulses) to be in step but shifted in time if one or the other were to receive spurious signals from some noise source. Realizing this, a re-examination of the VTCW data during this anomalous period results in the following scenario: beginning with frame 028 the VTCW had a nine bit shift; that is, the first nine bits of the code were actually the last nine bits of the code for the previous frame. The remaining bits were the first twenty-three bits of the proper VTCW for that frame.

This is particularly evident in frame 032 where the last bit of the code changed to a one. This is actually bit 23 of the real VTCW. This bit changed in the same frame in which the first five bits were all ones, the last five bits of the real time code belonging in the previous frame. These bits did not change to all zeros until the next frame.

It then becomes obvious that the PCM encoder sent its enable gate and shift pulses nine bits before the TDU generated its parallel load pulse. Under these circumstances, what was left in the VTCW shift register just before the start of the VTCW shift was a string of twenty-three ones

(automatically shifted into the front end of the shift register as the more significant bits were shifted out) and the last nine least significant bits from the previous frame, which were left in the register when the shift pulses ran out.

These nine bits were shifted out at the beginning of the new time code with gated shift pulses from the encoder. At this point the TDU loaded the VTCW register with the new count. What was in the shift register now was the proper time code word, with the most significant bit ready to be shifted out on the next shift pulse. The remaining twenty-three shift pulses from the encoder then shifted out the twenty-three most significant bits, leaving the nine least significant bits in the register, followed by a string of ones, to be shifted out when the next encoder enable gate and shift pulses were received.

The disruption must have been caused by a loss of counts equivalent to nine bits in the VTCW accumulator in the TDU, or a gain of the same number of equivalent counts in the encoder accumulator. One observation points to the latter. During the anomalous condition, the Universal Time tags, placed on the data tapes at the time of reception, are consistently 1 mS ahead of the expected data times. In other words, the PCM stream was shifted ahead by 1 mS during the VTCW disruption, and then shifted back 1 mS at master frame synchronization. The master frame synchronization did not take place until nine bits into main frame 000 of the new master frame.

The frame synchronization was re-established by frame 002 of the new master frame at UT 54749.522, 13.25 seconds after the first disrupted frame. The time code at this point was exactly as it would have been without the PCM disruption.

REFERENCES

1. Stevens, J.R.; and Vampola, A.L.: Description of the Space Test Program P78-2 Spacecraft and Payloads. SAMSO TR-78-24, Space and Missle Systems Organization, October 31, 1978.

2. Inouye, G.T.; and Sellen, J.M., Jr.: A Proposed Mechanism for the Initiation and Propagation of Dielectric Surface Discharges. Proc. 1978 Symposium on Effects of the Ionosphere on Space and Terrestrial Systems.

3. Langmuir, Irving; and Mott-Smith, Harold, Jr.: Studies of Electric Discharges in Gases at Low Pressures. General Electric Review XXVII, July-Dec. 1924; rpt. in The Collected Works of Irving Langmuir, Vol. 4, ed. C. Guy Suits, Pergamon Press, 1961, p. 31.

4. Chappell, C.R.: Recent Satellite Measurements of the Morphology and Dynamics of the Plasmasphere. Rev. Geophys. Space Phys.,10, 951, 1972, pp. 951-979.

5. Gussenhoven, M.S.; Hardy, D.A.; and Burke, W.J.: DMSF/F2 Electron Observations of Equatorward Auroral Boundaries and Their Relationship to Magnetospheric Electric Fields. J. Geophys. Res., to be published, 1981.

6. Lennartsson, Walter; and Reasoner, David L.: Low Energy Plasma Observations at Synchronous Orbit. J. Geophys. Res., 83, 1978, pp. 2145-2156.

TABLE 1. SELECTED P78-2 INSTRUMENTS

Instrument	Name	Use During Pass 89.4
SC1-1,-2, and -3	Surface Potential Monitors	Measure the charging potentials and currents of various materials.
SC1-7	R.F. Electromagnetic Wave Analyzer	Measures Electromagnetic (EM) emissions from 2 MHz to 30 MHz.
SC1-8A	Very Low Frequency (VLF) Wave Analyzer	Measures EM emission in the ELF, VLF and LF ranges.
SC1-8B	Transient Pulse Shape Analyzer	Measures the shape of EM pulses in the time domain from 7 nsec to 3.7 msec.
SC2-1 and -2 Probes	Sheath Electric Fields	Measure the potential of a conducting sphere 3 meters from the spacecraft.
SC4-1	Satellite Electron Beam System	Eject electrons to charge/discharge the spacecraft frame.
SC4-2*	Satellite Positive Ion Beam System	Eject positive ions and/or electrons to charge/discharge the spacecraft frame.
SC5	Rapid Scan Particle Detector	Measure the charged particle flux incident to the spacecraft.
SC9	UCSD Charged Particle Experiment	Measure the charged particle flux incident to the spacecraft.
SC10-3	Electric Field Detector	Measure the potential of a conducting cylinder at between 30 and 50 meters from the spacecraft.
SC11	Magnetic Field Monitor	Measure the ambient magnetic field at 4 meters from the spacecraft.
ML12-7	Spacecraft Contamination	Measure electron current to spacecraft.
TPM	Transient Pulse Monitor	Detect and measure electromagnetic pulses.

* Not used during Pass 89.4.

TABLE 2. INSTRUMENT "LINE-OF-SIGHT" ANGLES

Instrument	Alpha (degrees)	Beta (degrees)
SC1-1	307.5	0
SC1-2	120.	0
SC2-1 Boom	327.2	0
SC2-2 Boom	147.3	0
SC4-1	189.7	0
SC4-2	4.5	304
SC5 Parallel Detector	227.	90
SC5 Perpendicular Detector	227.	0
SC10-2 Boom	304.	0
SC10-3 Boom	124.	0
ML12-7	128.3	90

TABLE 3. SC4-1 MODES

Mode #	Time Start	Time Stop	Eb (keV)	Ib (mA)	Vsc (V)	Notes
1	52971	53745	0	0	5.7	Power off
2	53745	53894	0	0	6.0	Power on
3	53894	54082	0.3	0.1	5.7	
4	54082	54326	0.3	0.1	264.	Cap opened
5	54326	54437	1.5	0.1	1400.	
6	54437	54509	1.5	1.0	1440.	
7	54509	54542	1.5	1.0	-	Pulsed Beam
8	54542	54556	0.5	1.0	-	Pulsed Beam
9	54556	54651	0.5	1.0	480.	
10	54651	54728	0.5	6.0	480.	
11	54728	54809	3.0	6.0	2920.	SC2 damaged; occurrence of telemetry anomaly
12	54809	54820	1.5	6.0	1400.	
13	54820	55058	1.5	13.	1280.	
14	55058	55122	1.5	0.01	80.	
15	55122	55463	3.0	0.01	80.-	
16	55463	55535	0.5	0.01	8.1	
17	55535	55548	3.0	0.01	14.	
18	55548	55658	3.0	0.1	2880.	
19	55658	55707	0.3	0.1	192.	
20	55707	55857	0	0	0	Power off
21	55857	55869	0	0	0	Power on
22	55869	56269	0.3	0.01	268.	
23	56269	56368	0	0	-	Beam off

TABLE 3. SC4-1 MODES (Continued)

Mode #	Time Start	Time Stop	Eb (keV)	Ib (mA)	Vsc (V)	Notes
24	56368	56409	0.3	0.1	270.	
25	56409	56507	0.3	0.01	33.-93.	
26	56507	56519	1.5	0.01	62.	
27	56519	56638	1.5	0.1	1440.	
28	56638	56680	1.5	1.0	1440.	
29	56680	56692	3.0	1.0	2960.	
30	56692	56955	3.0	0.01	400.	
31	56955	56965	0.5	0.01	232.	
32	56965	56974	3.0	0.01	360.	
33	56974	57109	3.0	0.1	2894.	
34	57109	57609	0	0	-320.	Power Off

Table 4. SPACECRAFT FRAME POTENTIALS, SC5 AND SC10

Mode #	Eb (keV)	Ib (mA)	Vsc SC10 (kV)	Vsc SC5 (kV)
15	3.0	0.01	0.09 ± 0.01	0.1 ± 0.15
16	0.5	0.01	0.01	0.1 ± 0.05
18	3.0	0.1	2.88	2.4 ± 0.3
19	0.3	0.1	0.19	0.3 ± 0.1
30	3.0	0.01	0.4	0.3 ± 0.1
33	3.0	0.1	2.89	2.7 ± 0.5

TABLE 5. VEHICLE RESPONSE TO ELECTRON BEAM EJECTION (Vsc/Eb)

Ib (mA)	Eb(keV) 3.0 Vsc/Eb	1.5 Vsc/Eb	0.5 Vsc/Eb	0.3 Vsc/Eb
0.01	*0.03 **0.13	0.004	*0.016 **0.46	0.16
0.1	0.97	0.95	-	*0.64 **0.90
1.0	0.98	0.96	0.96	-
6.0	0.98	0.93	-	-
13.	-	0.85	-	-

*Sunlight

**Eclipse

TABLE 6. SAMPLE SURFACE POTENTIALS DURING MODE 11

Sample Number	Sample	(V)* Average Volts	(V+Vsc)** Maximum Volts
1V1	Aluminized Kapton	-102	2842
1V3	Optical Solar Reflecting Mirror	-42	2906
2V2	Alumized Kapton	-1189	1616
2V4	Conducting Reference Band	-258	2649

*Relative to spacecraft frame

**Relative to ambient plasma

TABLE 7. PULSE SENSORS

Sensor Name	Sensor Position	Measurement Type	Threshold (for 89.4)
TPM Low Z	Vehicle center tube Main vehicle wiring	Voltage	0.12 Volts
TPM High Z	Vehicle Center tube Main vehicle wiring	Voltage	2.40 Volts
TPM Solar	Solar Array to Power Conditioning Unit wire	Current	0.024 Amps
TPM Ground	Power Conditioning to Vehicle Frame wire	Current	0.84 Amps
SC1-8B #0 (Dipole)	External dipole on a 2 meter boom	Voltage	0.30V, 0.165V, 0.469V, 718V
SC1-8B #1 (CDU)	Loop antenna around Vehicle CDU	Voltage	" " " "
SC1-8B #2 (Harness)	Laid along a "typical" cable	Voltage	" " " "
SC1-8B #3 (Command)	Digital Command line from the CDU to SC1-8B	Voltage	" " " "
SC1-7 (RF analyzer)	SC10 dipole antennas 1.8m monopole on boom	RF (2 to 30 MHz)	-110 dBm

TABLE 8. COMPARISON OF PULSES FOR HIGH POWER SC4-1 MODES

Mode#	Eb (keV)	Ib (mA)	Total Pulses TPM	Total Pulses SC1-8	Pulses/Second TPM	Pulses/Second SC1-8	Eclipse
11	3	6	64	71	0.79	0.88	No
13	1.5	13	113	82	0.47	0.34	No
29	3	1	8	0	0.67	0	Yes
33	3	0.1	29	18	0.21	0.13	Yes
18	3	0.1	3	4	0.03	0.04	No

Note: TPM at Pulse Analysis Threshold Level 3
SC1-8B at 0.165V Pulse Analysis Threshold

Table 9. A COMPARISON OF SC10 AND SC2 PROBE VOLTAGES

Mode #	Time Start	Time Stop	Eb (keV)	Ib (mA)	-V10 (kV)	-V21 (kV)	-V22 (kV)	V21/V10	V22/V10
4	54082	54326	0.3	0.1	0.264	0.187	0.186	0.71	0.70
5	54326	54437	1.5	0.1	1.400	0.380	0.339	0.27	0.24
6	54437	54509	1.5	1.0	1.440	0.399	0.337	0.28	0.23
9	54556	54651	0.5	1.0	0.480	0.322	0.336	0.67	0.70
10	54651	54728	0.5	6.0	0.480	0.350	0.349	0.72	0.72
11	54728	54809	3.0	6.0	2.96	-	0.550	-	0.18

TABLE 10. MAGNETIC PITCH ANGLE AND SUN ANGLE CALCULATIONS

Period 1 (54728-54730, SC4-1 to 3 keV at 6 mA, SC2-1 probe failure)

Instrument	Time	Pitch Angle Degrees	Sun Angle Degrees
SC2-1 Boom	54728	13.2	146.5
	54729	14.1	152.7
	54730	17.4	158.9
SC2-2 Boom	54728	166.9	33.4
	54729	165.8	27.2
	54730	162.5	21.0
ML12-7	54728	103.1	86.6
	54729	103.1	86.6
	54730	103.1	86.6

Period 2 (54736, loss of telemetry sync)

Instrument	Pitch Angle Degrees	Sun Angle Degrees
SC2-1 Boom	50.3	162.9
SC2-2 Boom	129.6	17.3
SC4-1	88.6	59.4
ML12-7	103.3	86.6

Period 3 (54758-54759, SC2-2 probe failure)

Instrument	Time	Pitch Angle Degrees	Sun Angle Degrees
SC2-1 Boom	54758	164.5	25.4
	54759	160.9	19.2
SC2-2 Boom	54758	15.6	154.8
	54759	19.2	160.9
SC4-1	54758	50.7	162.2
	54759	56.7	156.0
ML12-7	54758	104.0	86.0
	54759	104.1	86.0

TABLE 11. SHADOWING ANGLES

Period 1 (SC2-1 failure)

Shadow entry sun angle = 165.5°
Half-shadow sun angle = 166.8°
Total shadow sun angle = 168.1°

SC2-1 Boom sun angle = 146.5° to 158.9°

Period 3 (SC2-2 failure)

Shadow entry sun angle = 165.3°
Half-shadow sun angle = 166.6°
Total shadow sun angle = 167.9°

SC2-2 Boom sun angle = 154.8° to 160.9°

TABLE 12. TABLE OF SC2 FAILURE PARAMETERS

Current away from outer sphere (electrons)	> 200 μA
Potential of current source (negative)	≤ 1500 V
Voltage to which follower output is driven	-1400 V
Total input charge required	2 μC (max.)
Time required	10 mS at 200 μA to 100 μS at 20 mA
Charge available to destroy string	2 μC

Table No. 13 Pass 89-4 PCM Encoder Output for VTCW, Frame Counter, and Synchronization Words During Anomalous Condition.

Frame	UT (Sec.)	Vehicle Time Code Word (Words 000,001,002,003)	Frame Ctr (Word 124)	Synchronization (Words 125,126,127)
020	54735.772	00100110111011001000100010100100	00010100	000001001100111101011111
021	54735.897	00100110111011001000100010101101	00010101	000001001100111101011111
022	54736.022	00100110111011001000100010111001	00010110	000001001100111101011111
023	54736.147	00100110111011001000100010111111	00010111	000001001100111101011111
024	54736.272	00100110111011001000100011000000	00011000	000001001100111101011111
025	54736.397	00100110111011001000100011001001	00001001	100111101011111111111111
026	54736.522	00100110111011001000100000000000	00001001	100111100000110100000000
027	54736.646	10100010000100110111011001000100	00011011	000001001100111101011111
028	54736.771	11011001100100110111011001000100	00011100	000001001100111101011111
029	54736.896	11100010000100110111011001000100	00011101	000001001100111101011111
030	54737.021	11101010100100110111011001000100	00011110	000001001100111101011111
031	54737.146	11110011000100110111011001000100	00011111	000001001100111101011111
032	54737.271	11111011100100110111011001000100	00100000	000001001100111101011111
033	54737.396	00000000000100110111011001000100	00100001	000001001100111101011111
034	54737.521	00001000100100110111011001000100	00100010	000001001100111101011111
120	54748.271	10111011100100110111011001000101	01111000	000001001100111101011111
121	54748.396	11000000000100110111011001000101	01111001	000001001100111101011111
122	54748.521	11001000100100110111011001000101	01111010	000001001100111101011111
123	54748.646	11010001000100110111011001000101	01111011	000001001100111101011111
124	54748.771	11011001100100110111011001000101	01111100	000001001100111101011111
125	54748.896	11100010000100110111011001000101	01111101	000001001100111101011111
126	54749.021	11101010100100110111011001000101	01111110	000001001100111101011111
127	54749.146	11110011000100110111011001000101	01111111	000001001100111101011111
000	54749.271	11111011100100110111011000000000	00000000	000000000000001001100111
001	54749.396	10101111010000000000000000000000	00000000	110010010000000000000000
002	54749.522	00100110111011001000110000010000	00000010	000001001100111101011111
003	54749.647	00100110111011001000110000011011	00000011	000001001100111101011111
004	54749.772	00100110111011001000110000010000	00000100	000001001100111101011111
005	54740.897	00100110111011001000110000010101	00000101	000001001100111101011111
006	54750.022	00100110111011001000110000011001	00000110	000001001100111101011111
007	54750.147	00100110111011001000110000011111	00000111	000001001100111101011111

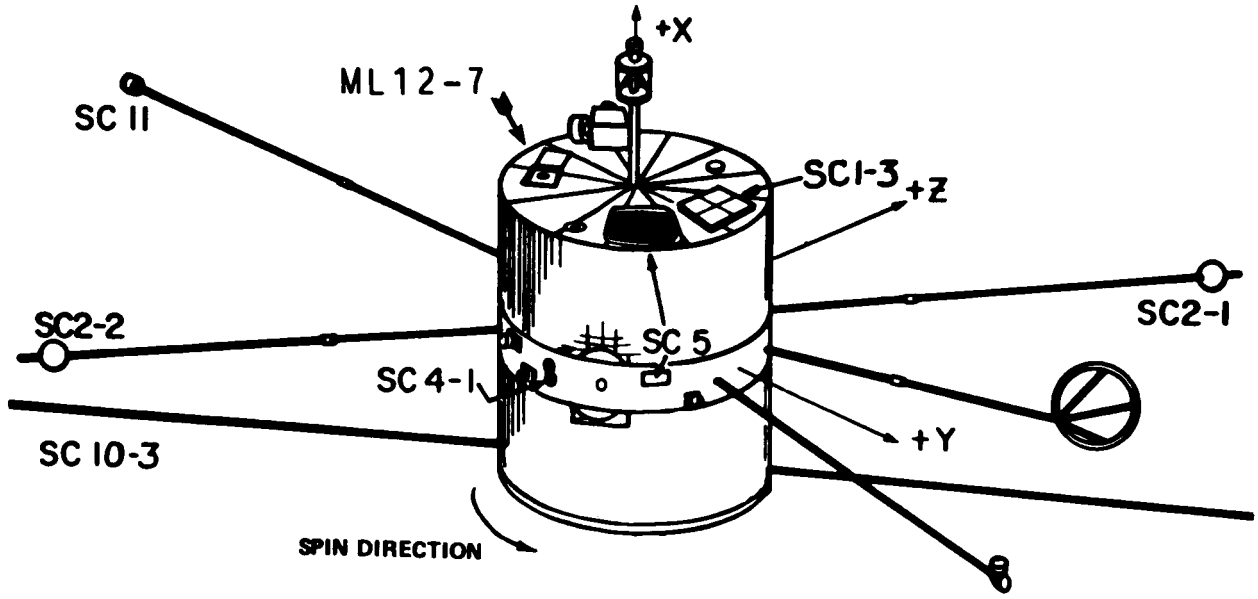

Fig. 1 P78-2

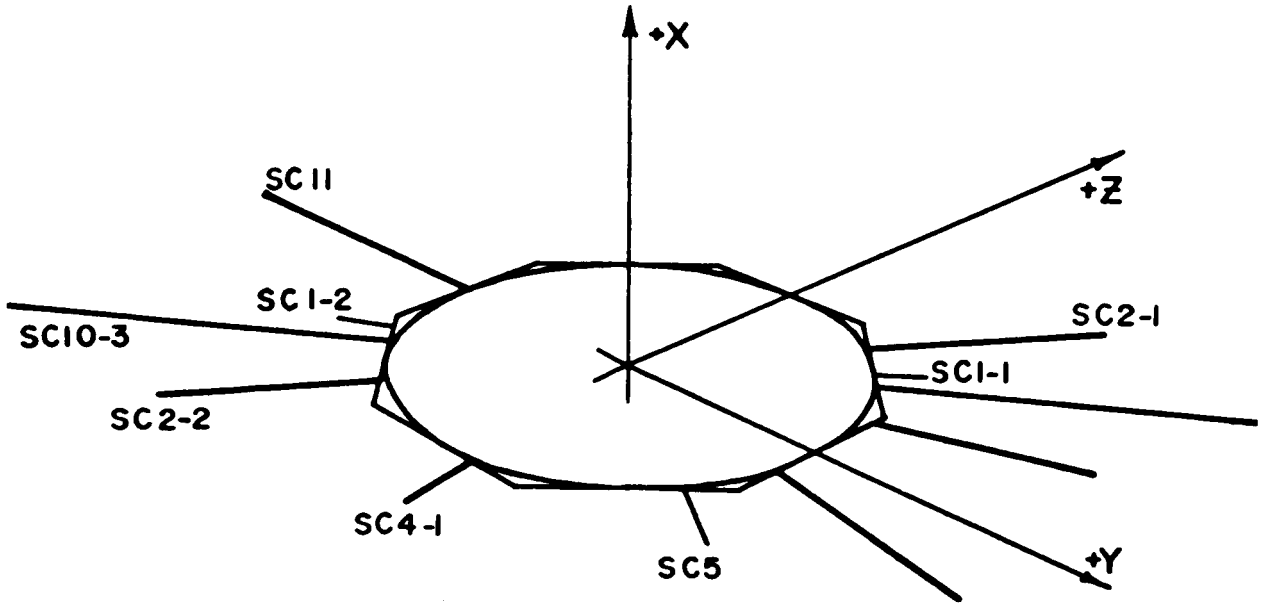

Fig. 2A P78-2 Relative Instrument Angles

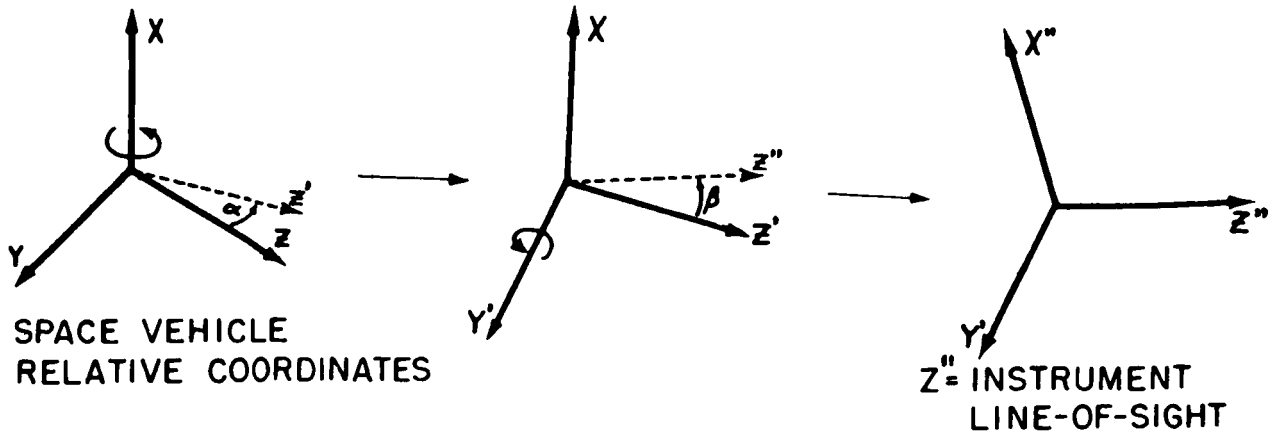

Fig. 2B Space Vehicle Mount Angle Definition

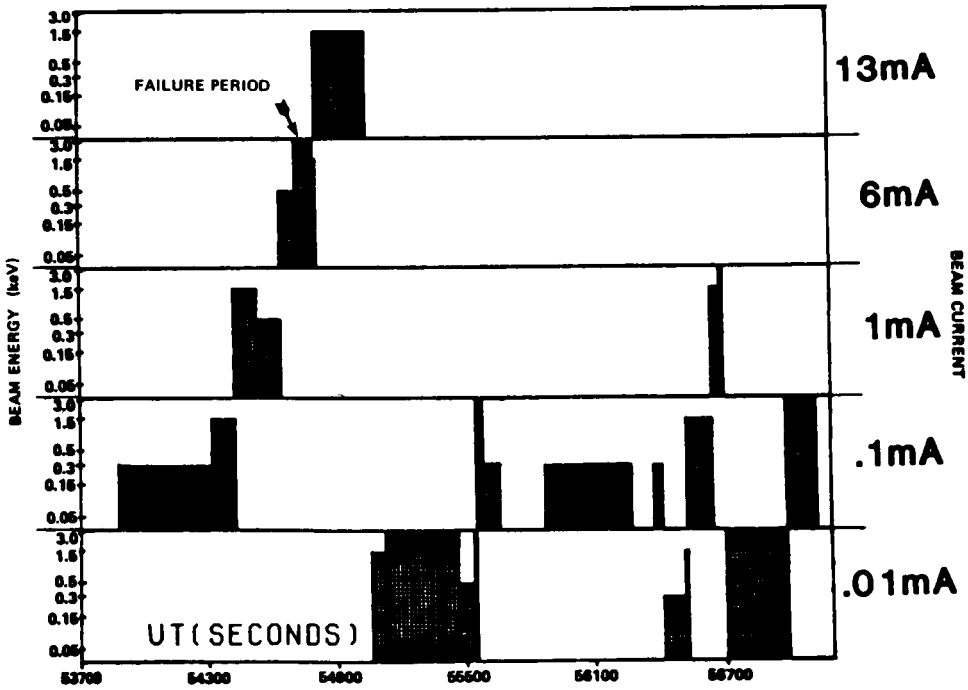

Fig. 3 SC4-1 Operations - Pass 89.4

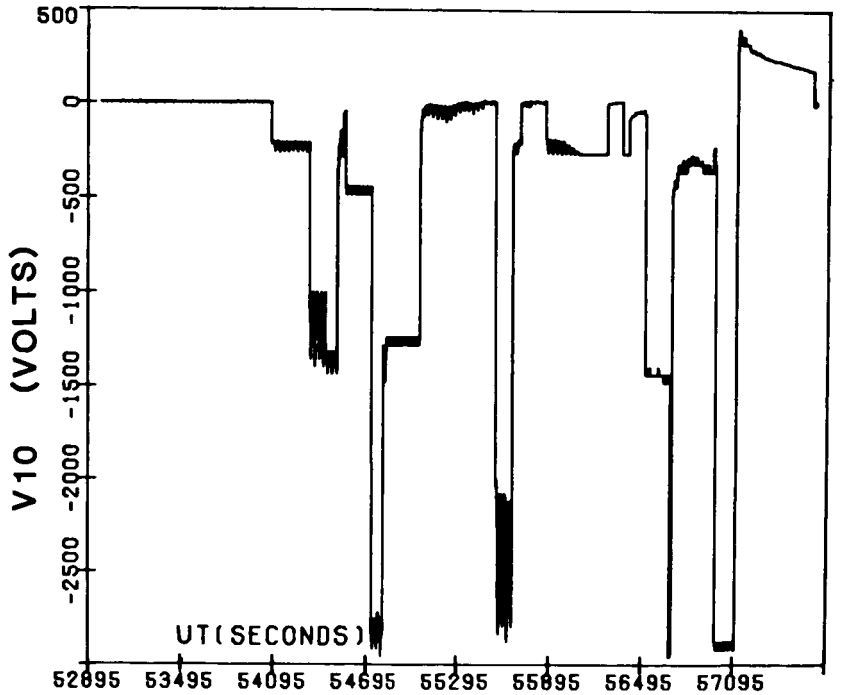

Fig. 4 SC10 Potential - Pass 89.4

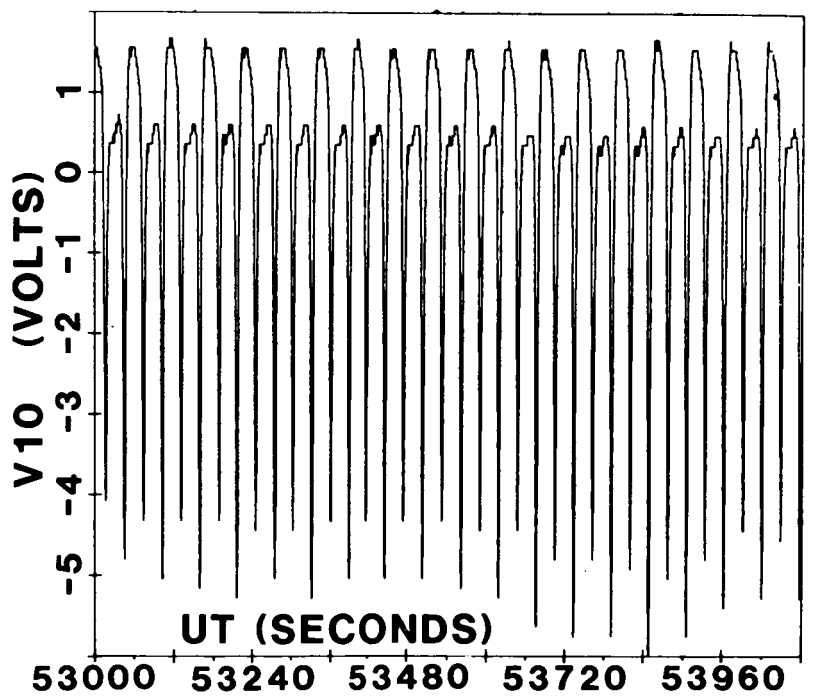

Fig. 5 SC10 Potential During Initial SC4-1 Operation Period

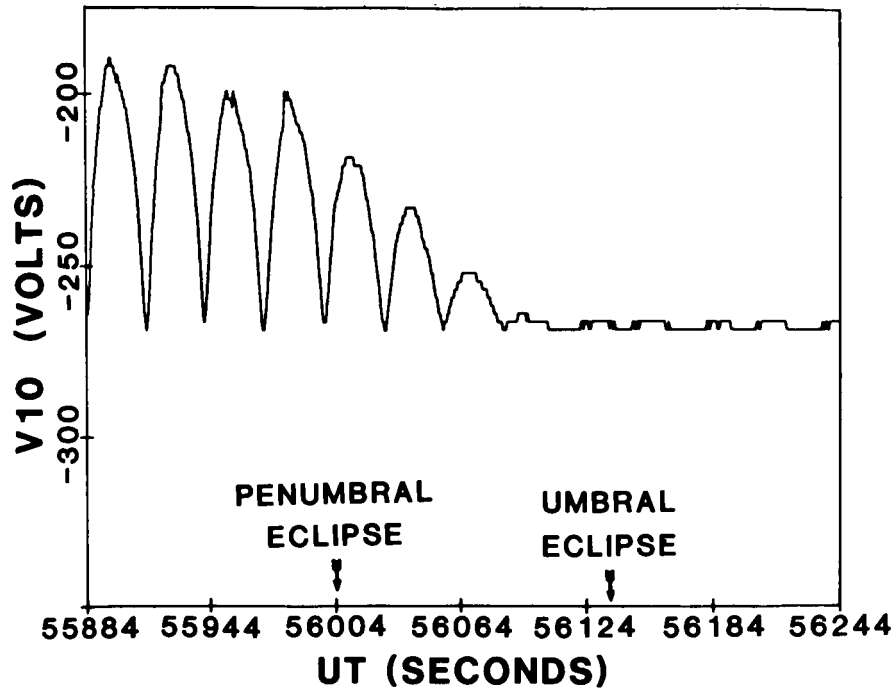

Fig. 6 SC10 Potential Entering Eclipse - Pass 89-4

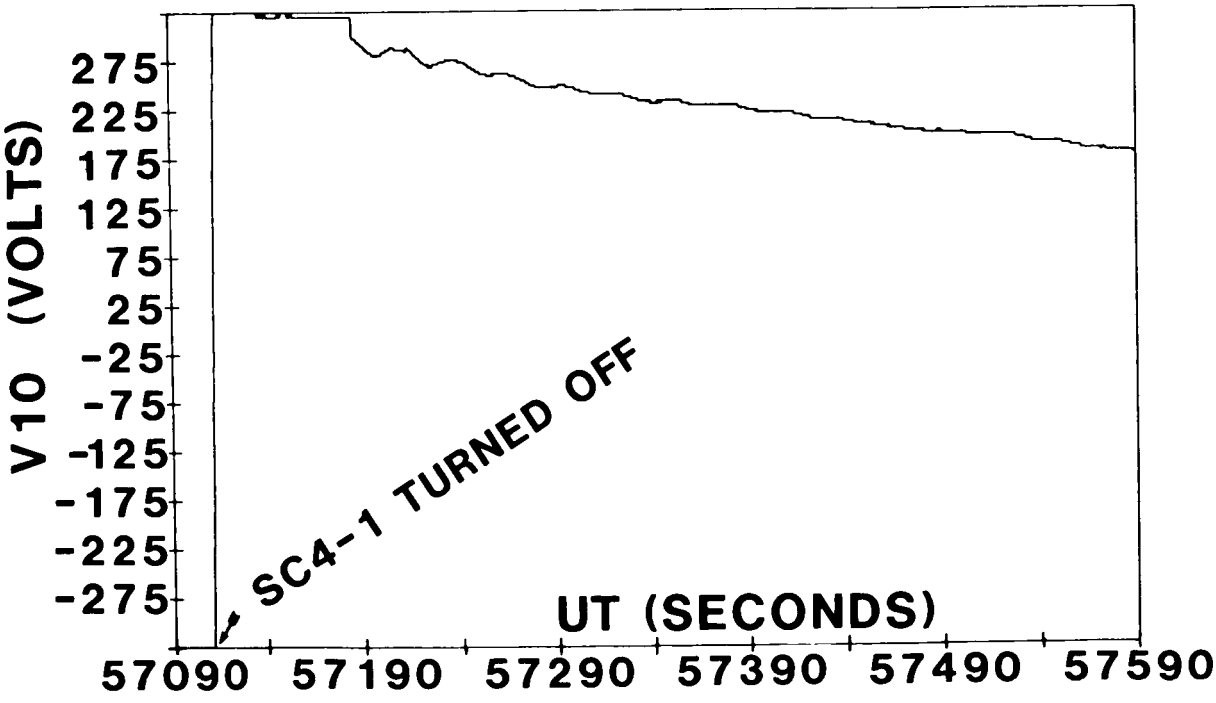

Fig. 7 SC10 Potential at SC4-1 Turn-Off

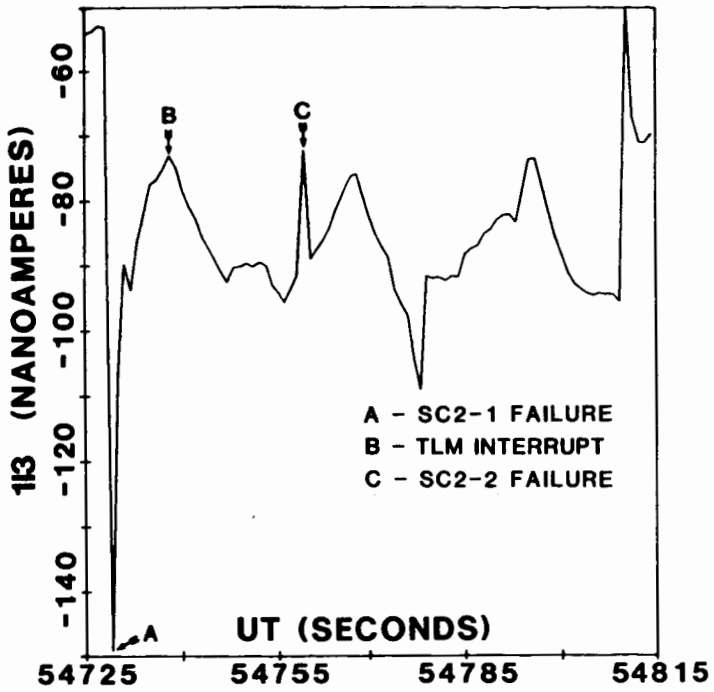

Fig. 8 SPM Current Through Optical Solar Reflector - SC4-1 Mode 11

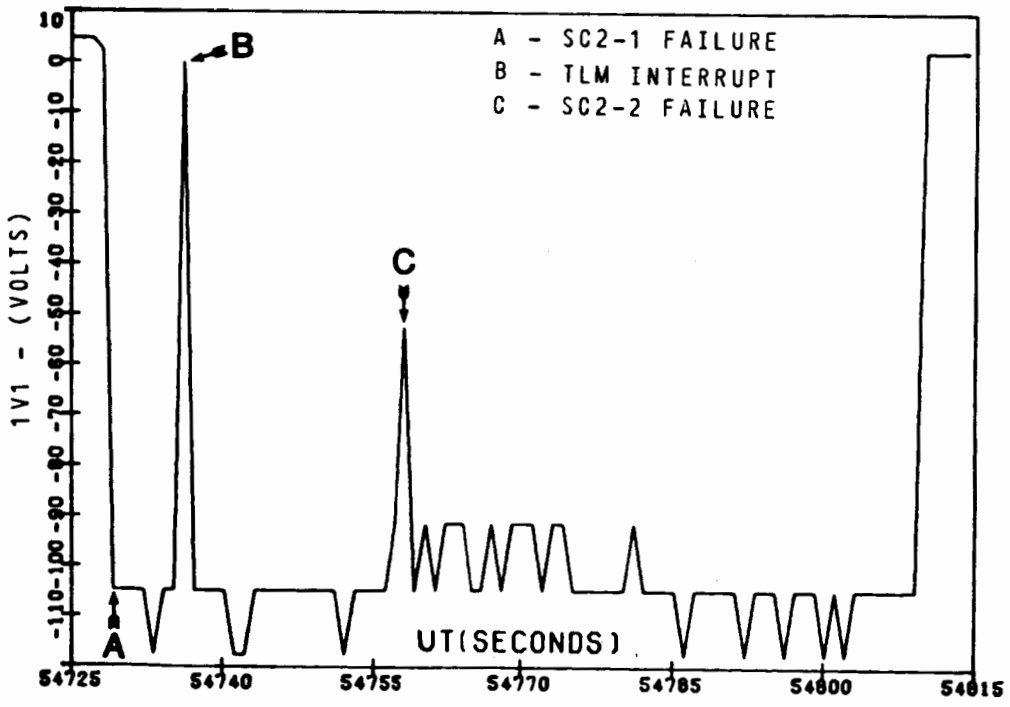

Fig. 9 SPM Front Surface Potential - Kapton Sample - SC4-1 Mode 11

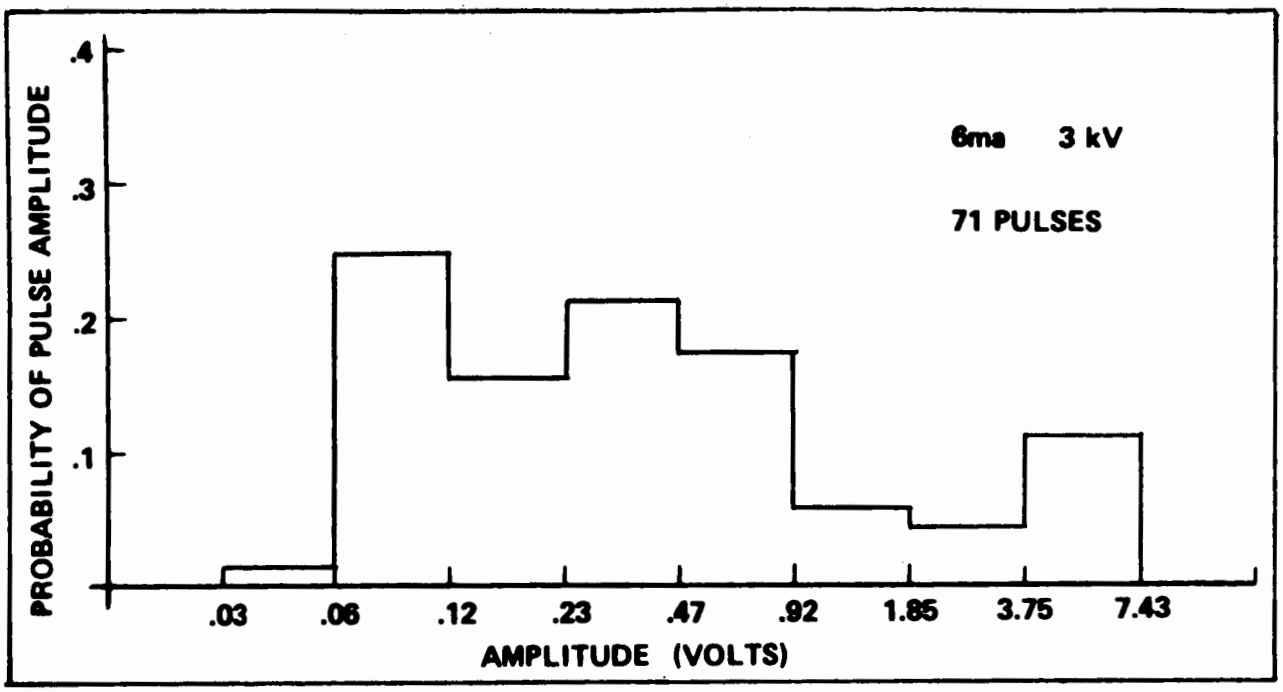

Fig. 10 Amplitude Distribution of SC1-8 Pulses Above Threshold #1

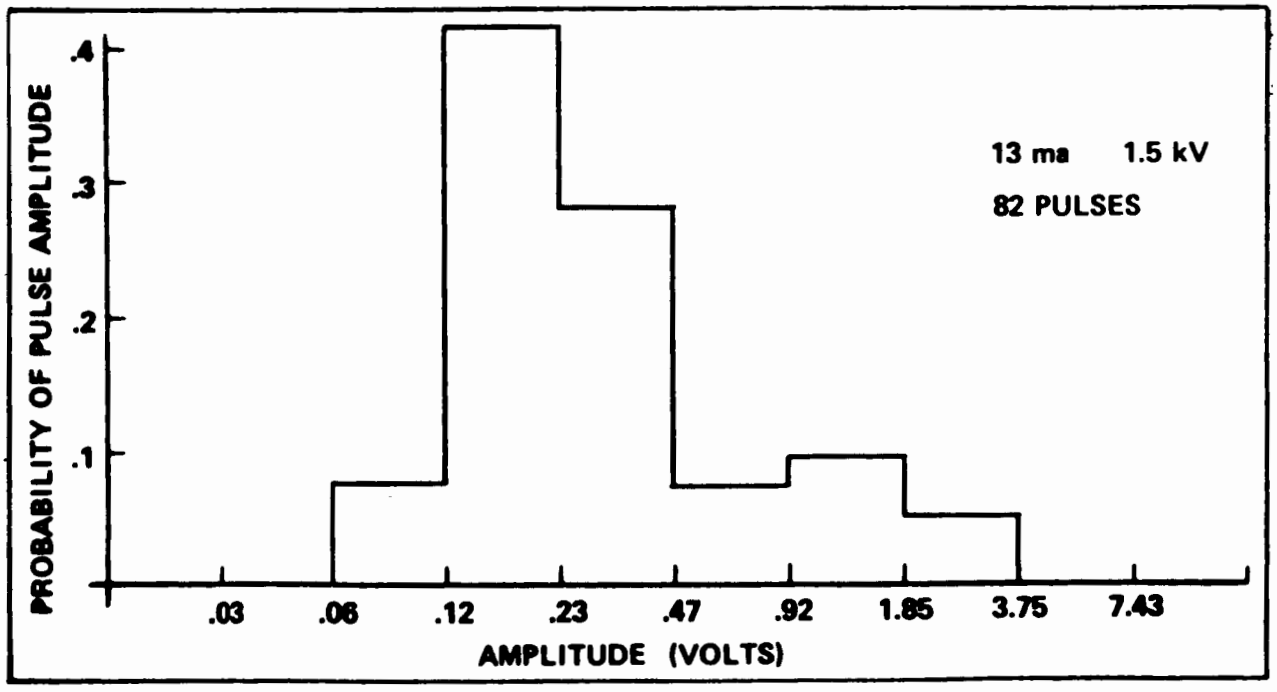

Fig. 11 Amplitude Distribution of SC1-8 Pulses Above Threshold #2

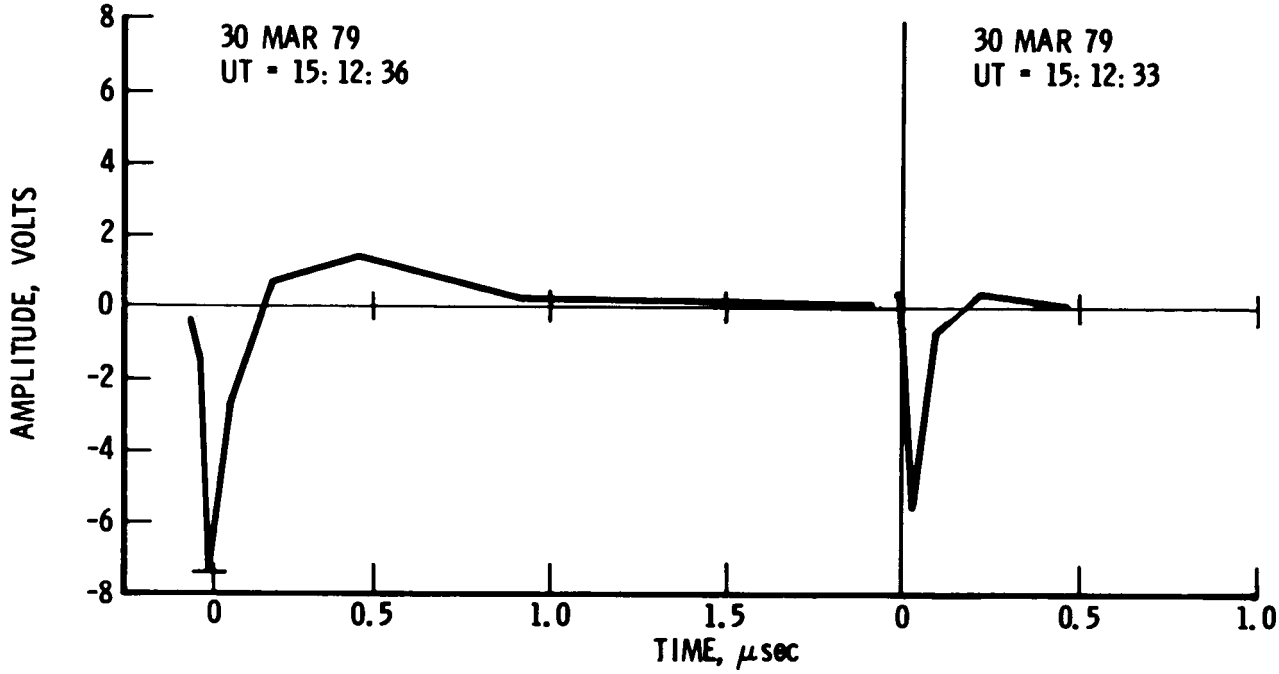

Fig. 12 SC1-8B Pulse Shape - External Dipole

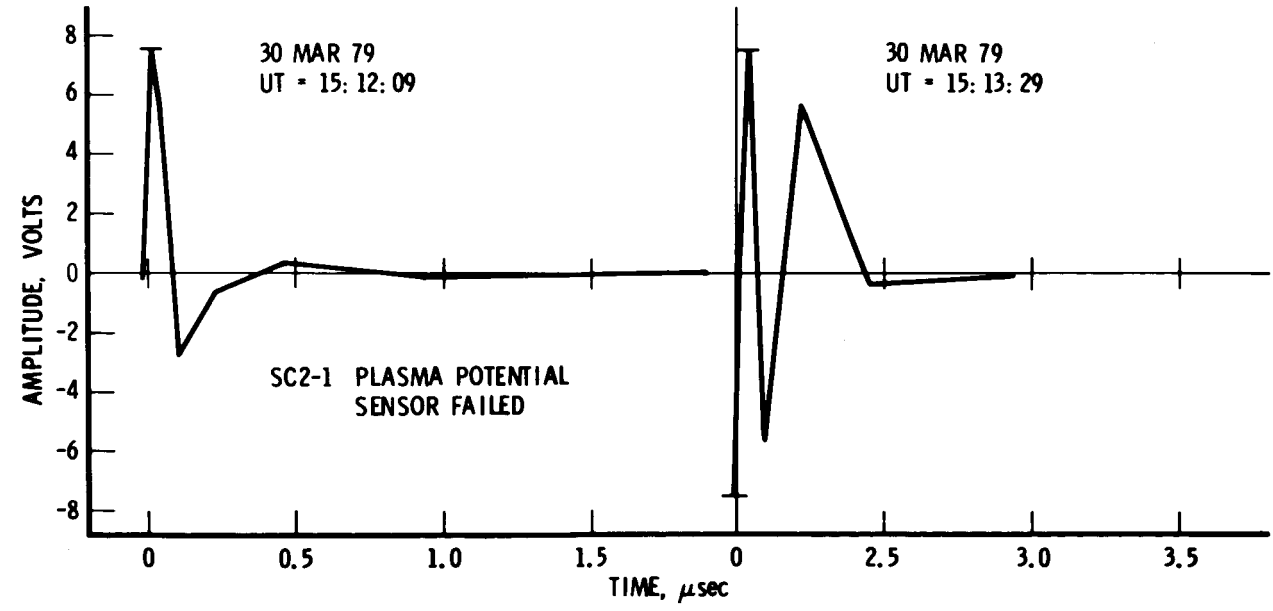

Fig. 13 SC1-8 Pulse Shape - Harness Wire

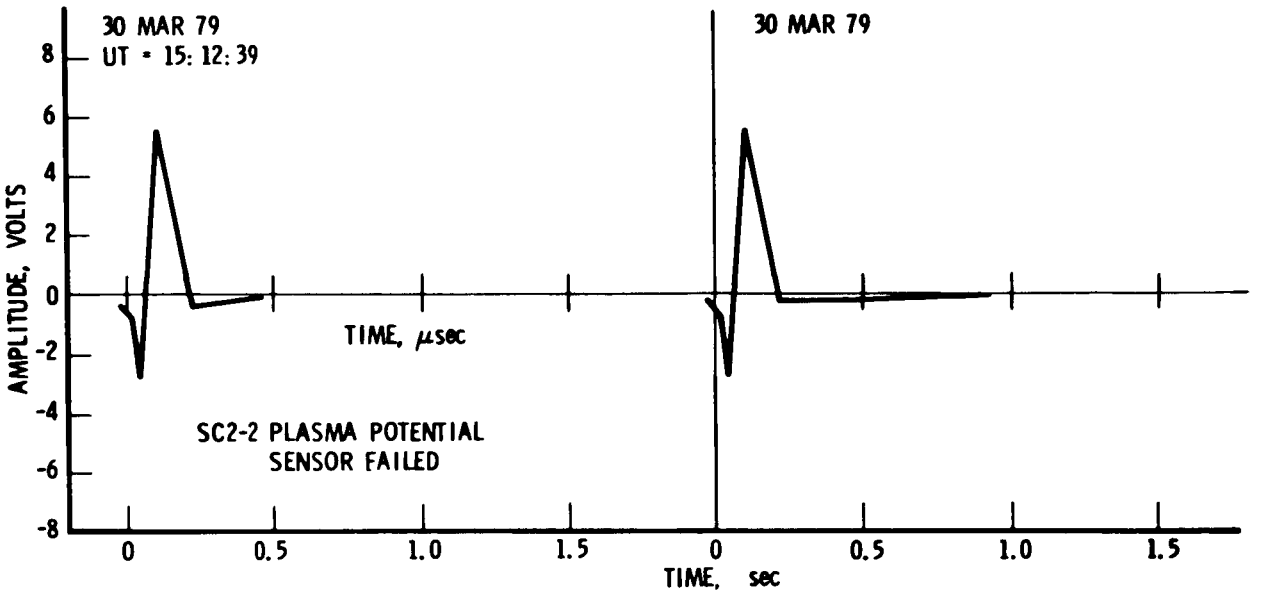

Fig. 14 SC1-8 Pulse Shape - CDU Loop

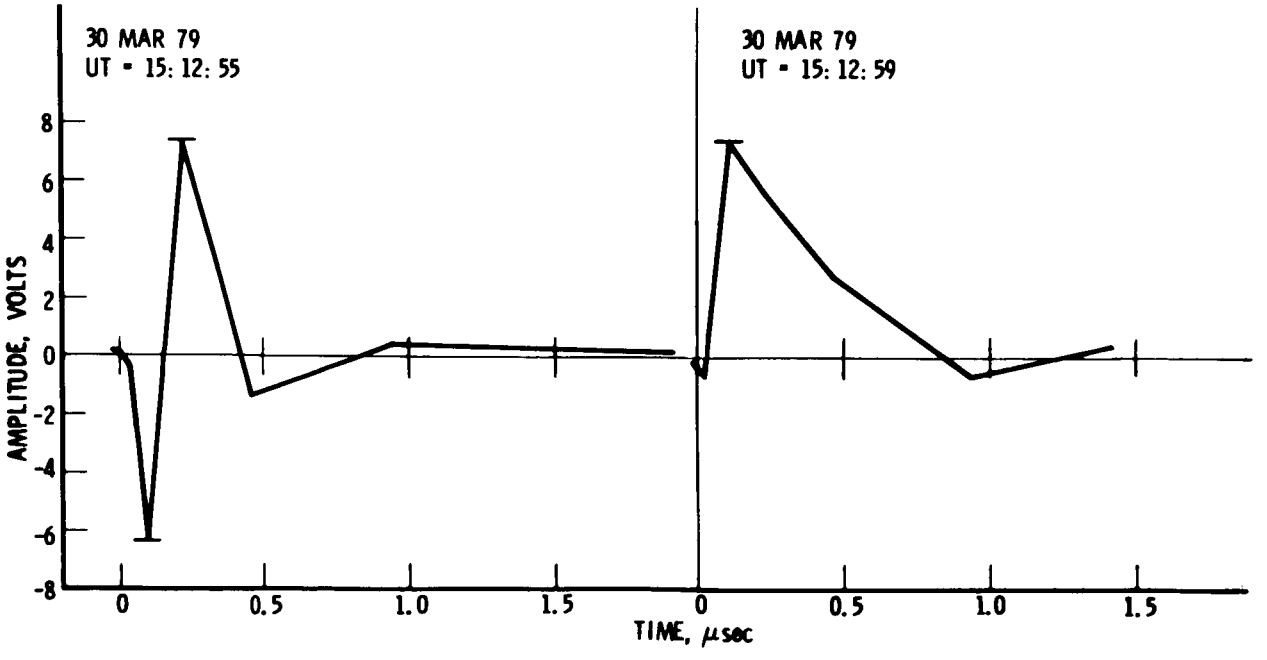

Fig. 15 SC1-8 Pulse Shape - Command Line

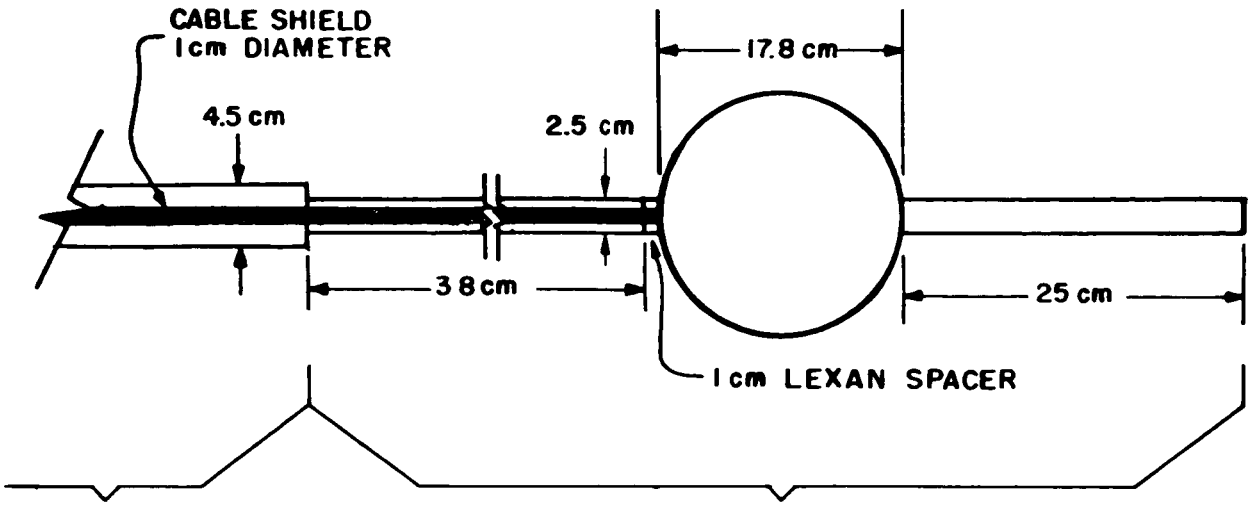

SC2 BOOM : 3 m LONG
KAPTON COVERED WITH
2.54 cm Pt BANDS,
0.635 cm SPACINGS

SC2-1,-2 : CONDUCTIVE COATING
(AQUADAG)

NOTE: CABLE SHIELD REMOVED LAST~8cm
BEFORE LEXAN SPACER

Fig. 16 SC2-1, -2 Experimental Geometry

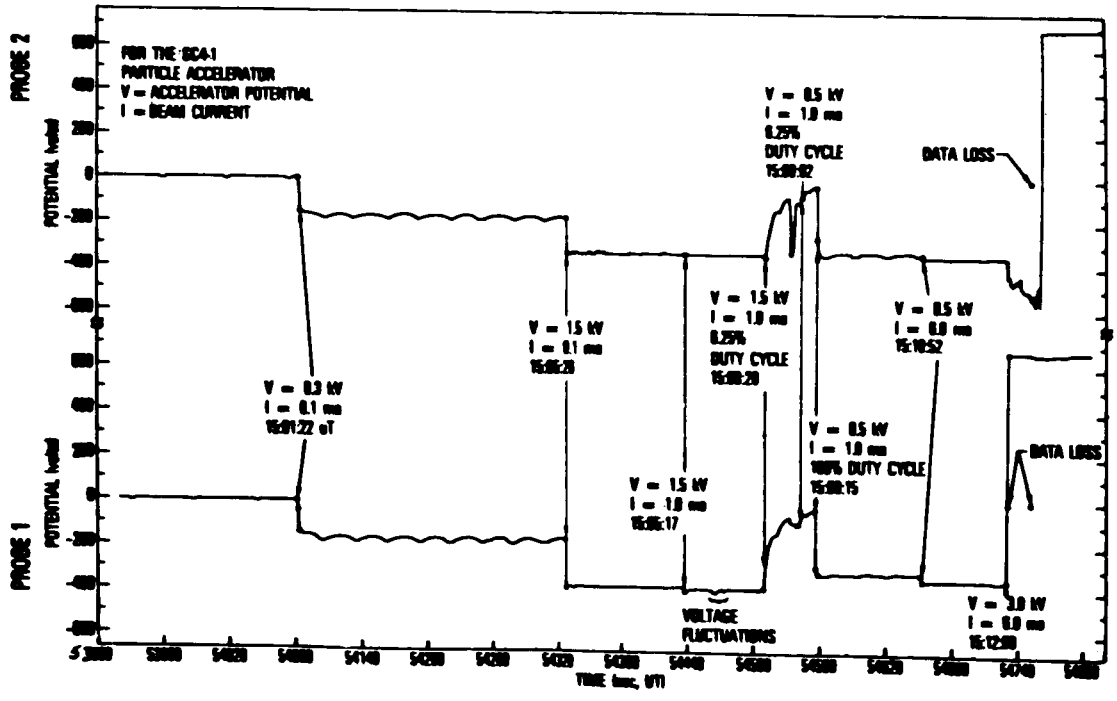

Fig. 17 SC2 Probe Voltages

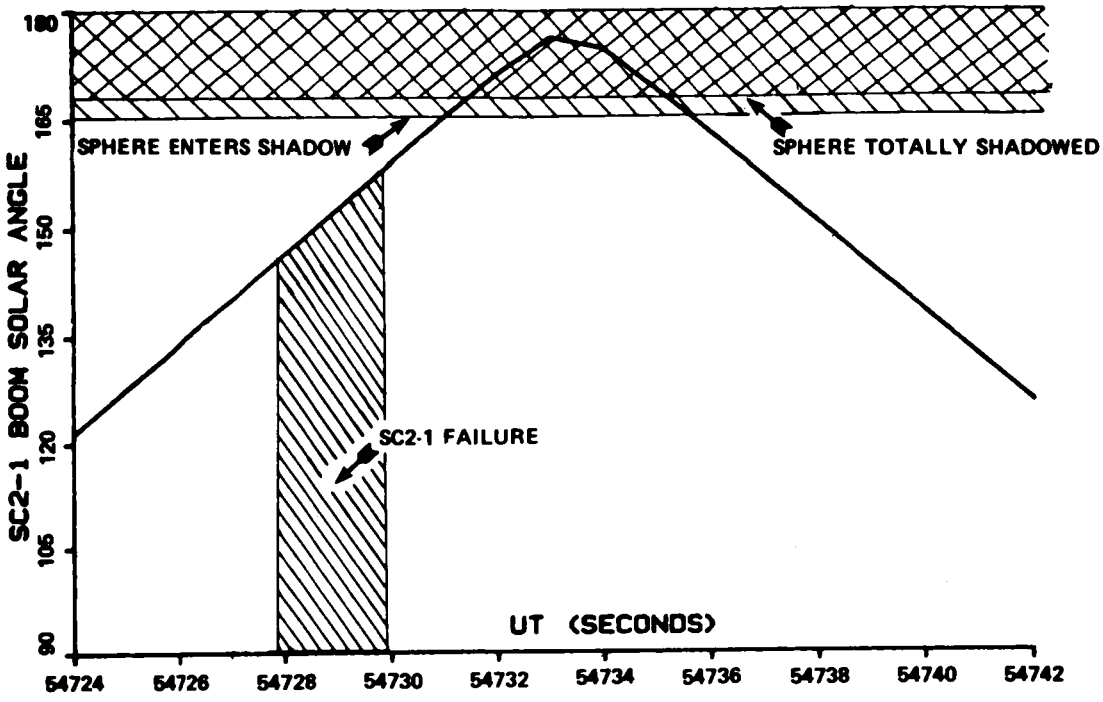

Fig. 18 SC2-1 Boom Solar Angle

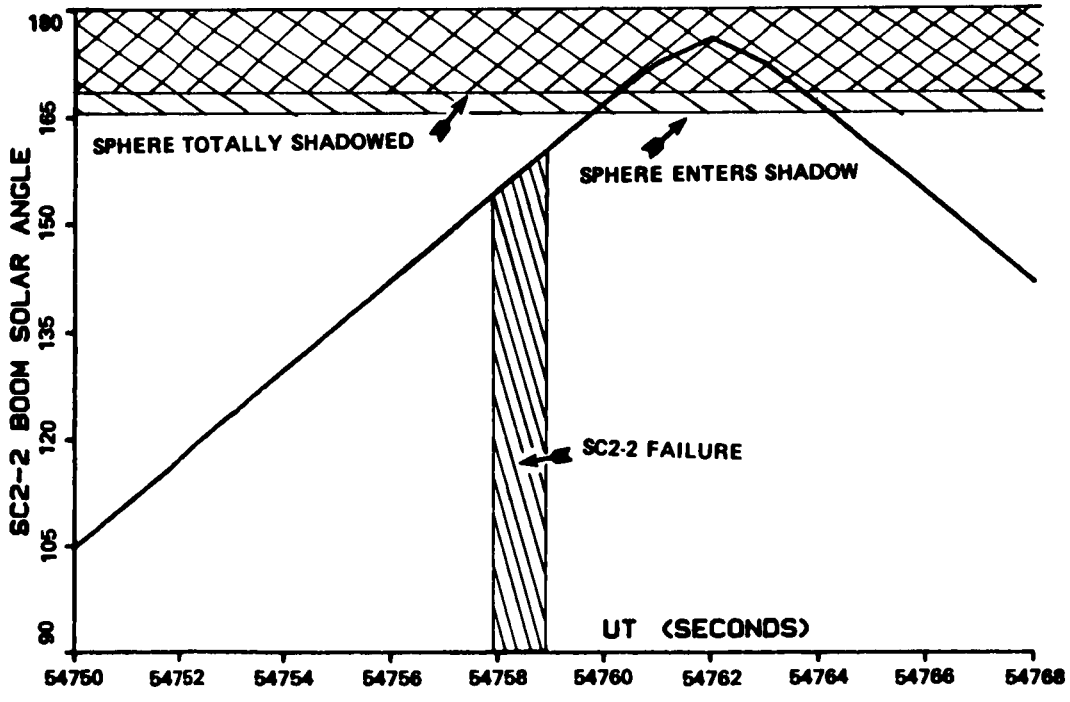

Fig. 19 SC2-2 Boom Solar Angle

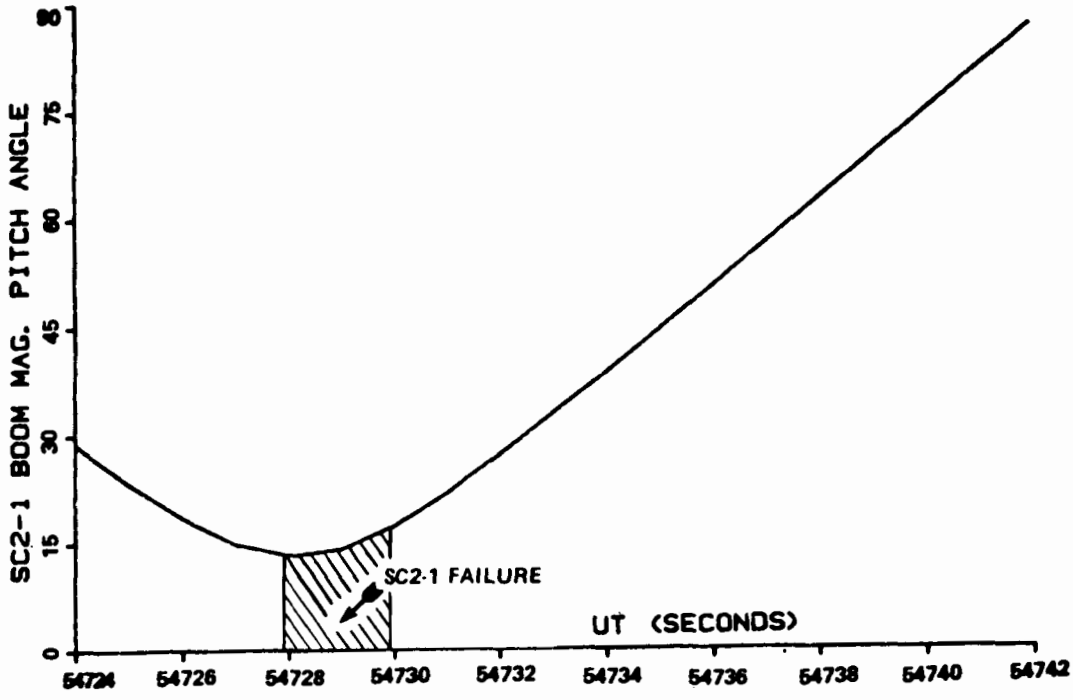

Fig. 20 SC2-1 Boom Magnetic Pitch Angle

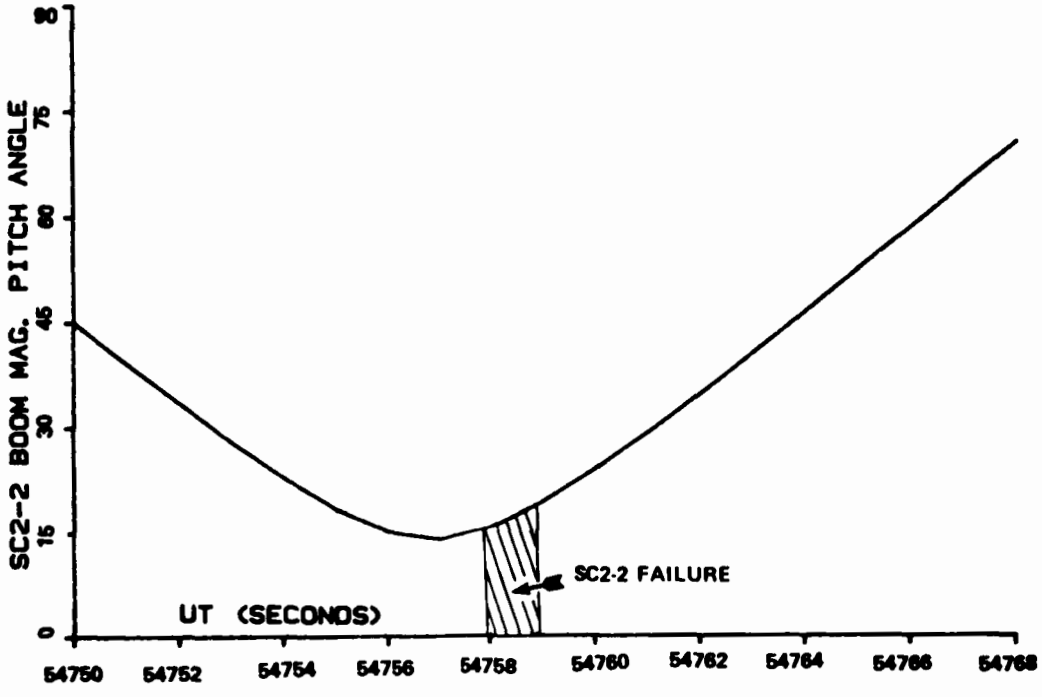

Fig. 21 SC2-2 Boom Magnetic Pitch Angle

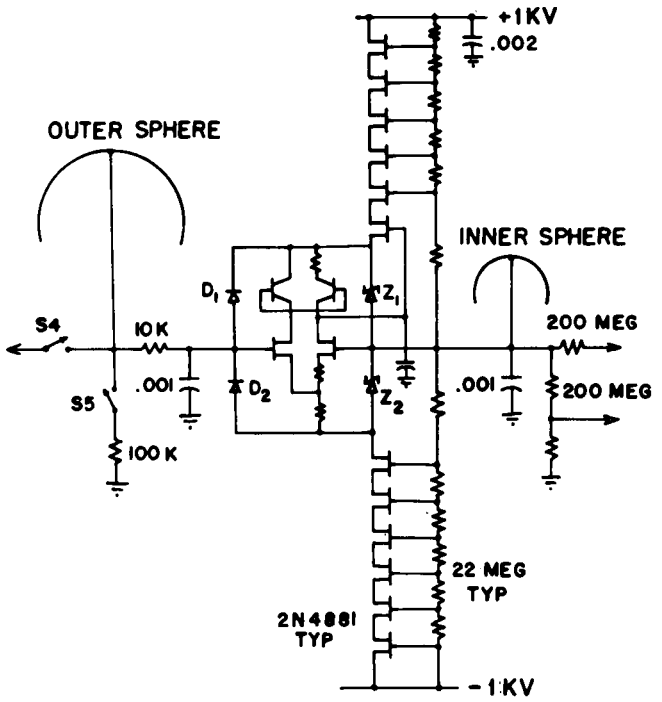

Fig. 22 SC2-1, -2 Voltage Follower Circuit

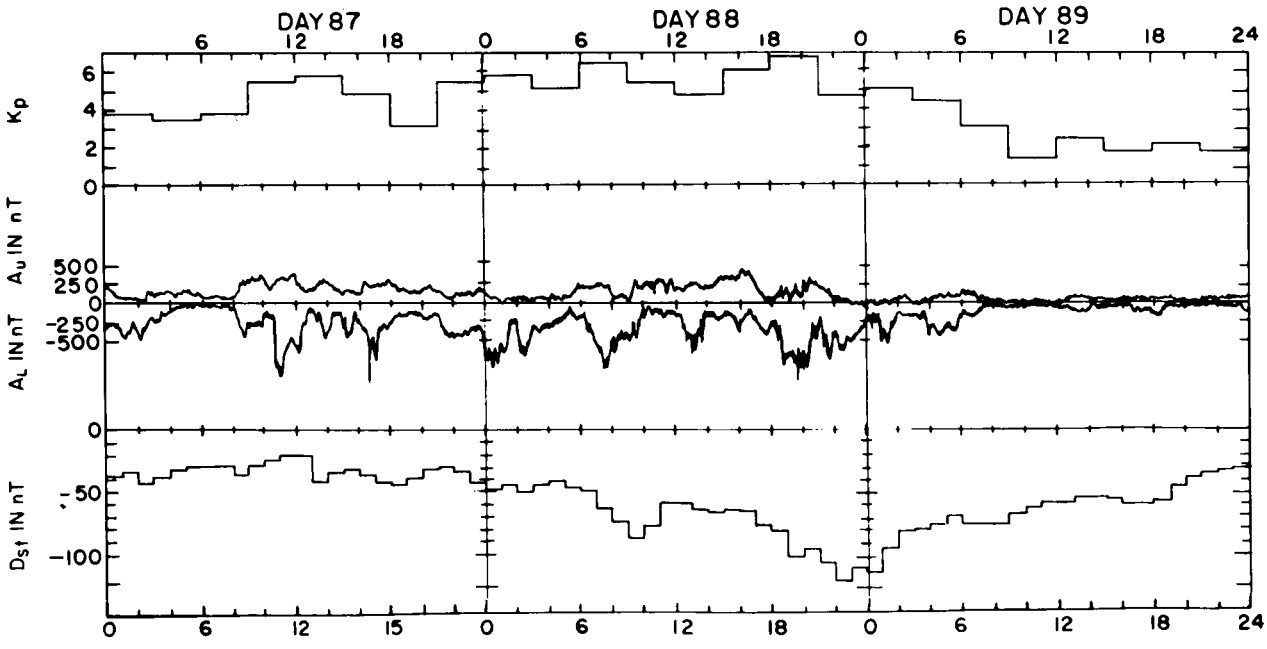

Fig. 23 Magnetic activity indices, March 28-30, 1979

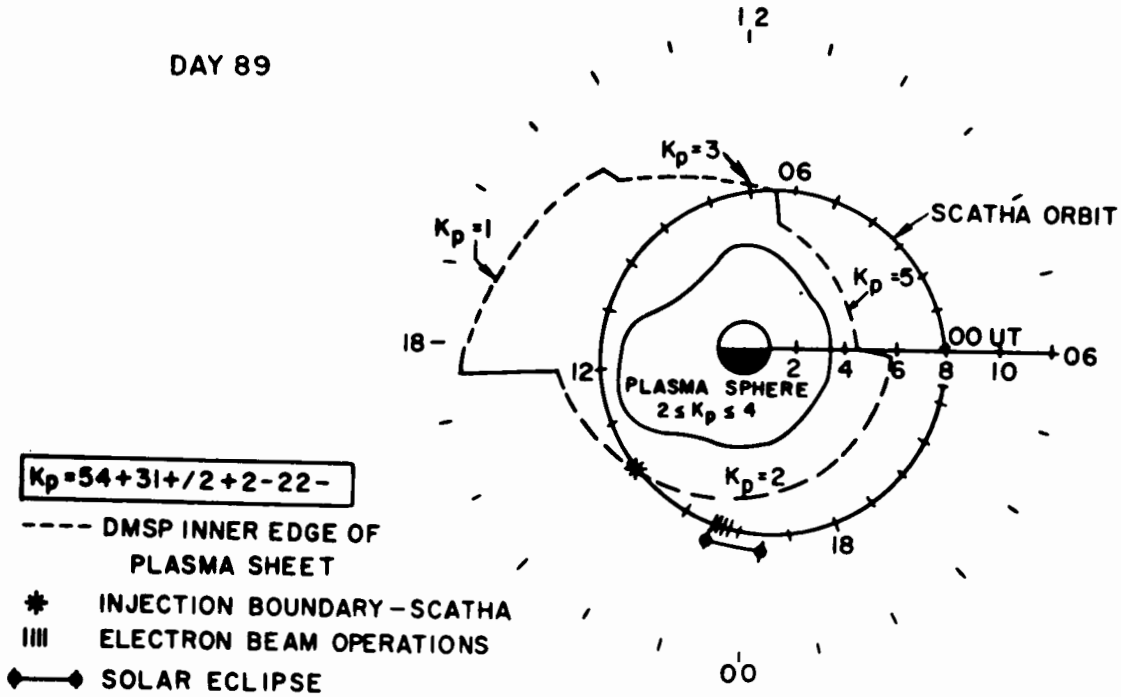

Fig. 24 The SCATHA orbit for March 30, 1979, with plasmasphere and plasma sheet (dashed lines) boundaries.

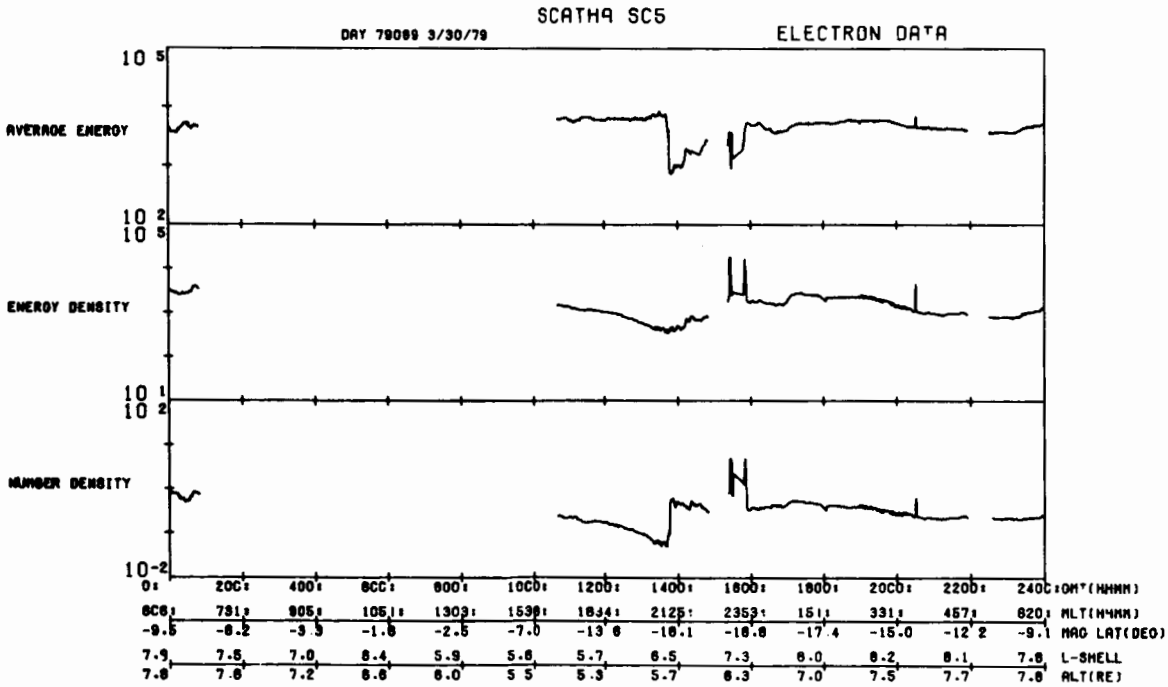

Fig. 25 Electron parameters, measured by SC5, in the energy range .05-60 keV, for March 30, 1979.

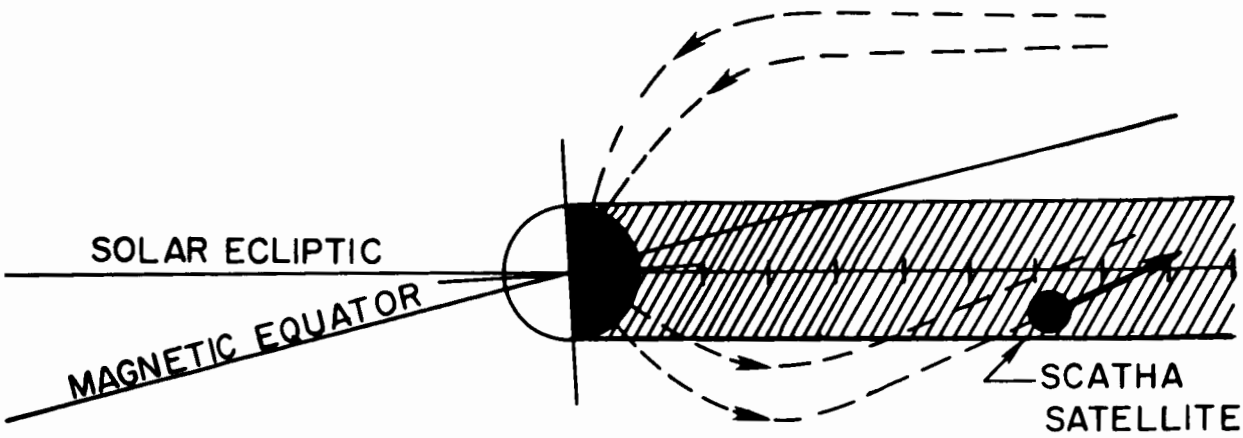

Fig. 26 Schematic diagram of the SCATHA position and the magnetic field direction during pass 89.4.

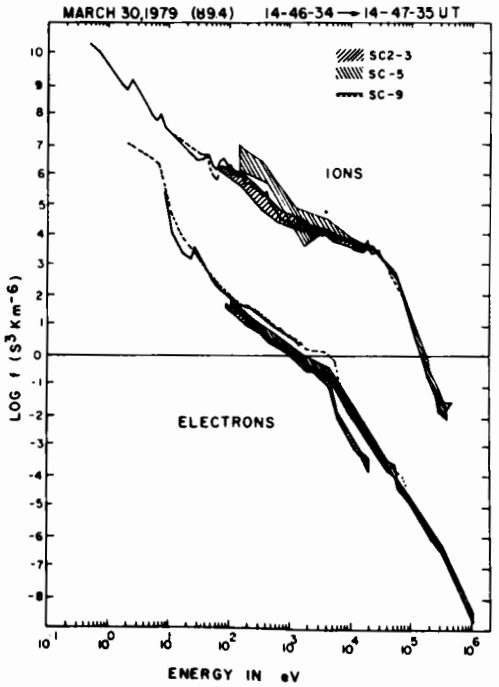

Fig. 27 Distribution functions of electrons and ions measured by SC2-3, SC5 and SC9 on March 30, 1979, at 14:47 UT.

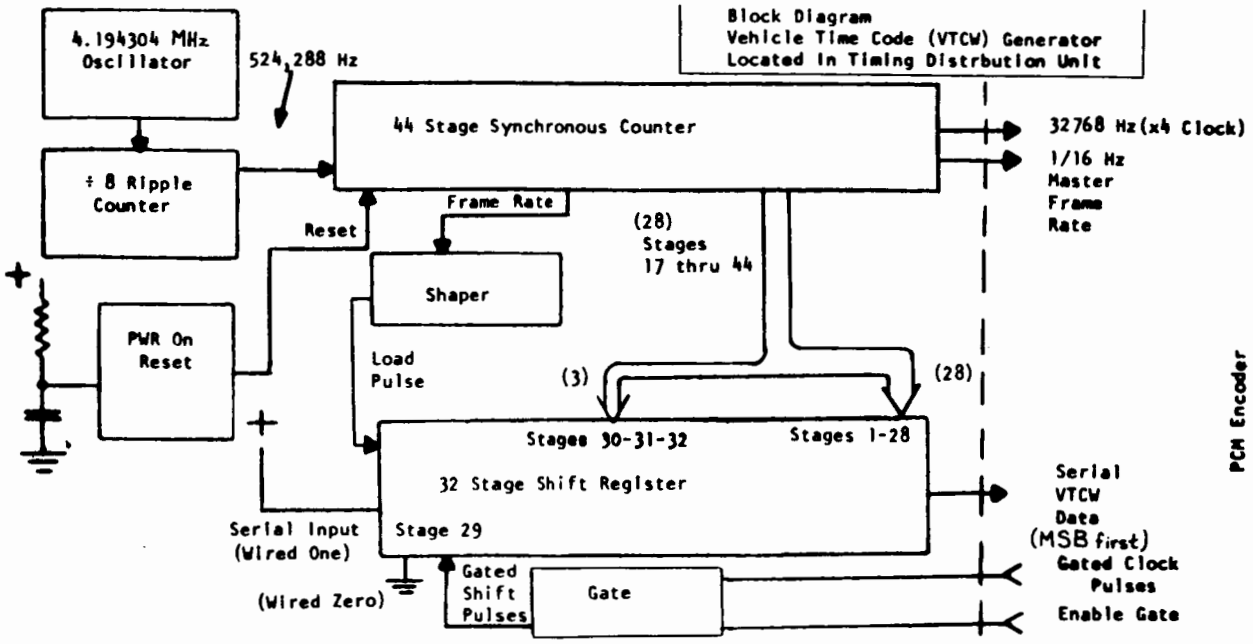

Fig. 28 Vehicle Time Code (VTCW) Generator

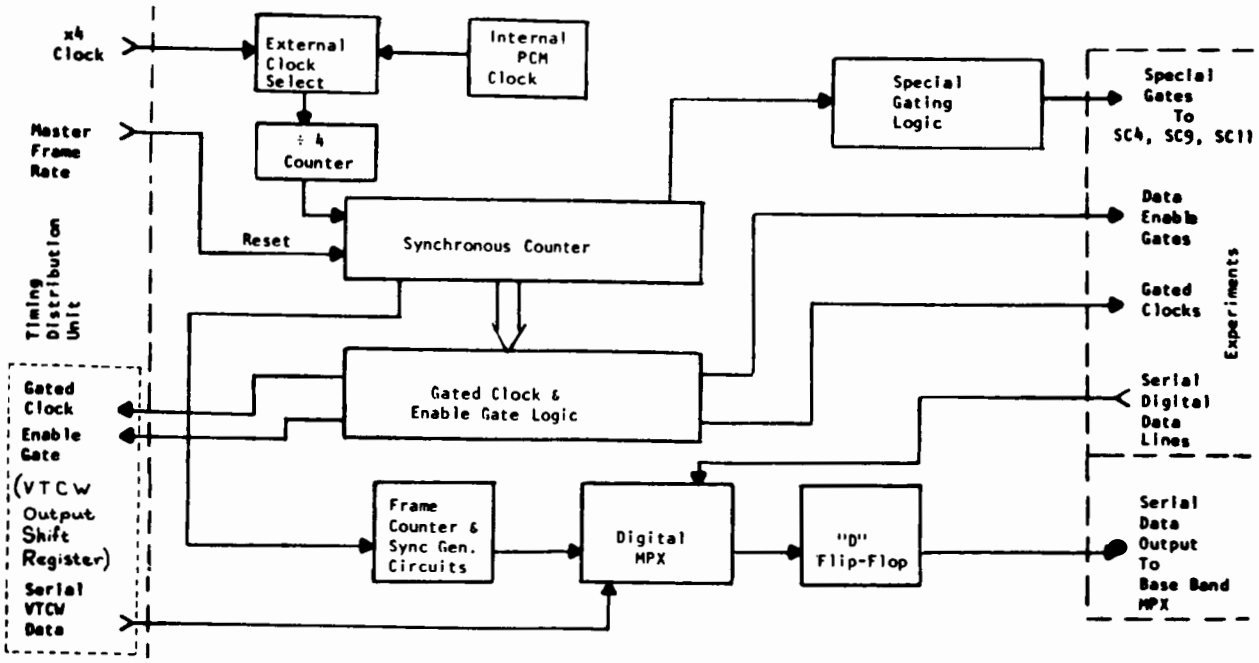

Fig. 29 PCM Encoder - Block Diagram